# Investigation of Forging Performance for AA6082

**Ozkan Tunc**

Ditas Dogan Yedek Parca Imalat and Teknik A.S

**Ilyas Kacar** ( ✉ ikacar@gmail.com )

Nigde Ömer Halisdemir Üniversitesi   https://orcid.org/0000-0002-5887-8807

**Fahrettin Ozturk**

Ankara Yildirim Beyazit University

---

---

# Investigation of forging performance for AA6082

Ozkan Tunc[1] iD, Ilyas Kacar[2*] iD, Fahrettin Ozturk[3,4] iD

[1] Ditas Dogan Yedek Parca Imalat and Teknik A.S., Nigde, Turkey.

[2] Mechatronics Engineering Department, Nigde Omer Halisdemir University, Nigde, Turkey.

[3] Mechanical Engineering Department, Ankara Yildirim Beyazit University, Ankara, Turkey.

[4] Turkish Aerospace Industries, Inc., Ankara, Turkey.

## Abstract

6XXX series aluminum alloys are generally excellent alternatives to steels for many forged parts in aerospace and automotive industries. In this study, the forging performance of the 6082 aluminum alloy is investigated in order to replace the existing material for forged steel parts. The effect of artificial aging of the alloy on the microstructure and mechanical properties is studied. Optimum aging conditions are determined. Results reveal that AA6082 could be a good replacement for applications where shock and vibrational loads exist. The rod end part currently manufactured from AISI1045 can be replaced by AA6082 without any design changes. The major drawback is that the cold forging of the aged alloy is poor due to its brittle nature and crack initiations. Therefore, warm or hot forging is recommended to overcome the poor forgeability.

**Keywords:** Al-Si alloy; AA6082; artificial aging; hot forging; fatigue; automotive.

* Corresponding author: ikacar@ohu.edu.tr, +90 388 225 46 48

# 1. INTRODUCTION

Reducing the fuel consumption and carbon dioxide emissions is a challenging issue in automotive industry. Design changes and using lighter materials are some strategies used by the car part manufacturers. 6082 aluminum alloy (AA6082) is a good candidate as an alternative material. Because it is lighter than steel and it is abundantly available among other aluminum alloys. Mechanical properties improved by aging process are comparable to the steels. Therefore, this alloy has the potential to be a good replacement for steel parts in the suspension, chassis, and engine. For example, in the aviation industry, the arms in the flight control mechanism and the brake bodies are often made of AA6082. However, due to the strict regulations in the aerospace and automotive industry, it is a problematic situation to determine whether a one-to-one replacement with the use of a new material is possible without changing the design of the part. A change in design can irrevocably lead to additional development time, proses, and expertise costs for the manufacturers since the part needs to meet the same set of requirements. It is well-known that trial and error process is not a cost effective method. Also an inverse engineering is often not possible since the applications are unique. Whether thermo-mechanical treatments can solve this problem is the primary scope of this study.

Aging is a time and temperature dependent heat treatment process. AA6082 is one of the suitable materials for artificial aging. Different aging conditions lead to different mechanical properties. AA6082 is often artificial aged at 160 °C, after dissolving at 500 °C [1]. While the tensile strength of AA6082-O which is not heat treated alloy is around 170 MPa, it can reach 427 MPa after aging [2]. However, the microstructure becomes brittle and its impact energy absorption ability decreases. On the other hand, the strength suffers when the forgeability increases [3]. It has been reported that both strength and forgeability decreases in the absence of dissolving [4]. Thus, a careful aging process design is needed to attain both high strength and high toughness together.

The forgeability of AA6082 is poor for cold forging due to crack initiations [5]. The forgeability increases at elevated temperatures up to 160 °C [6]. The forgeability can increase up to 159% with warm forging [7]. Grain recovery effects the deformability [8]. The process temperature of the hot forging acts as a dissolving process. The

artificial aging after the hot forging leads to a homogeneous grain distribution in the microstructure [9]. When hot billets without extrusion are forged directly, a homogeneous micro structure and a more economical forging are guaranteed [10].

The forgeability increases by increasing soaking duration due to the homogeneous distribution of the phases inside the microstructure at the dissolution stage [11-13]. A 15 minutes waiting time at 540 °C is suggested for dissolution [14]. Water is frequently used as a cooling medium. Fast cooling ensures the smaller-sized $Mg_2Si$ solid precipitates in the microstructure. Finer or distorted precipitates can cause the strength increase [15,16]. The $\beta''$-($Mg_5Si_6$) phase seen up to 300 °C is the main factor in increasing the strength. When it transforms into $\beta'$-($Mg_{1.8}Si$) and $\beta$-($Mg_2Si$), the strength decreases. Increasing the number of the solid precipitates in the microstructure makes the material brittle [17]. The $\beta''$ phase is rich in dislocations [18,19]. Increasing temperature decreases the number of dislocations [20].

The hardening behavior of the alloy is clearly seen during successive forgings [21]. It is important to define plastic deformation in simulations. The alloy is sensitive to deformation rate during forging, and its tensile strength increases at high strain rates [17].

AA6082 alloy presents high flexibility in terms of mechanical properties depending on the heat treatment and deformation conditions. The novelty of the work is that the optimum heat treatment conditions have been investigated to replace the material of the automotive rod end part. The part was manufactured by hot forging for AISI1045 steel, meanwhile AA6082-O (ISO: AlSi1MgMn) alloy has been investigated as a replacement of it. Replacing a structural part with the lighter one without sacrificing safety, manufacturing time, and low cost is of primary concern for the car part manufacturers. The effect of aging on the microstructure was also presented. Optimum values were used in fatigue and hot forging simulations. Press force requirement for forging, the burr ratio, the processing time, the residual stress, the deformation, and the service life of the rod end were compared.

## 2. MATERIAL AND EXPERIMENTS

Extruded rods with a 20 mm diameter were used for sample preparation. The compositions of AA6082-O and AISI1045 are given in Table 1. The chemical compositions are critical for the required heat treatment, the material microstructure, and the mechanical properties of the materials.

**Table 1** Chemical compositions of AA6082 and AISI1045 (wt.%)

| AISI 1045 | C | Si | Mn | P | Cu | Cr | Mo | Ni | Al | S | Sn |
|---|---|---|---|---|---|---|---|---|---|---|---|
| | 0.44 | 0.26 | 0.65 | 0.007 | 0.18 | 0.15 | 0.04 | 0.04 | 0.02 | 0.03 | 0.015 |
| AA 6082 | Mg | Si | Mn | Fe | Cu | Cr | Ti | Ni | Al | Zn | Co |
| | 0.99 | 3.54 | 1.84 | 1.44 | 3.76 | 1.39 | 0.68 | 2.38 | 72.69 | 2.62 | 1.96 |

## 2.1. Heating and cooling sequences

Heating temperature and duration, types of quenching medium, sequential treatments and soaking time were investigated. The alloy was heated up to the dissolution temperature at a heating rate of 36 °C/s. When the temperature reached the set value, the samples were kept for 2 - 10 hours inside the furnace. Then the samples were air cooled or quenched in water or water-polymer mixtures. The mixtures contained 25% polymer, 50% polymer, and 75% polymer, respectively. The dissolved samples were then artificially aged at 175 - 220 °C during 2-10 hours. The artificial aging process was also repeated sequentially for other samples. A scheme of the aging treatment is shown in Fig. 1. Quenching environments composed of 1%, 2%, 3%, 4%, 5%, 6%, 7%, 8% polymer-water mixtures were also investigated to determine their effects on the mechanical properties.
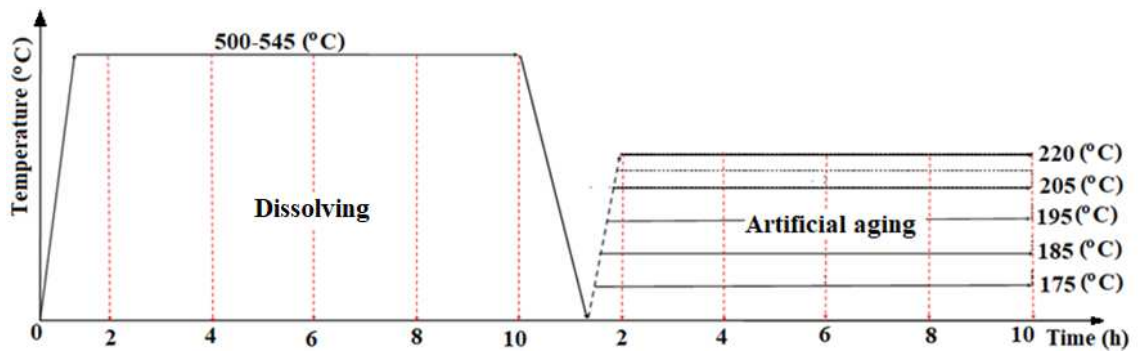


**Fig. 1** A scheme for the heat treatment cycle

4

The specimen designation for tests is summarized in Table 2. It also gives their ultimate tensile strength (UTS) and strain at break.

**Table 2** The specimen and their tensile results

| Test No. | Soaking temp. (°C) | Soaking duration (h) | Artificial aging temp. (°C) | Artificial aging duration (h) | Quenching | UTS (MPa) | Strain at break (%) |
|---|---|---|---|---|---|---|---|
| 0 (*) | - | - | - | - | - | 166 | 12.83 |
| 1 | 500 | 4 | - | - | Air | 204 | 9.12 |
| 2 | 500 | 6 | - | - | Air | 194 | 8.37 |
| 3 | 500 | 8 | - | - | Air | 218 | 9.69 |
| 4 | 500 | 10 | - | - | Air | 148 | 9.12 |
| 5 | 500 | 4 | - | - | Water | 238 | 8.16 |
| 6 | 500 | 6 | - | - | Water | 244 | 10.9 |
| 7 | 500 | 8 | - | - | Water | 242 | 10.69 |
| 8 | 500 | 10 | - | - | Water | 248 | 9.91 |
| 9 | 500 | 2 | 175 | 2 | Air | 218 | 9.88 |
| 10 | 500 | 2 | 175 | 2 | Water | 271 | 8.69 |
| 11 | 500 | 2 | 175 | 2 | Water | 232 | 8.79 |
| 12 | 500 | 2 | 175 | 2 | %25 polymer | 230 | 8.93 |
| 13 | 500 | 2 | 175 | 2 | %50 polymer | 217 | 10.03 |
| 14 | 500 | 2 | 185 | 2 | Air | 384 | 8.81 |
| 15 | 500 | 2 | 185 | 4 | Water | 249 | 5.96 |
| 16 | 500 | 2 | 185 | 4 | %25 Polymer | 272 | 7.06 |
| 17 | 500 | 2 | 185 | 4 | %50 polymer | 273 | 6.89 |
| **18** | **500** | **2** | **185** | **4** | **Air** | **406** | **7.42** |
| 19 | 500 | 2 | 185 | 6 | Air | 399 | 5.25 |
| 20 | 500 | 2 | 185 | 8 | Air | 391 | 3.64 |
| 21 | 500 | 2 | 185 | 10 | Air | 373 | 4.56 |
| 22 | 545 | 2 | 195 | 2 | Water | 386 | 6.89 |
| 23 | 545 | 2 | 195 | 4 | Water | 391 | 8.71 |
| 24 | 500 | 2 | 195 | 6 | Water | 257 | 7.71 |
| 25 | 500 | 2 | 195 | 6 | %25 polymer | 265 | 7.48 |
| 26 | 500 | 2 | 195 | 6 | %50 polymer | 268 | 3.90 |
| 27 | 545 | 2 | 195 | 6 | Water | 365 | 3.78 |
| 28 | 545 | 2 | 195 | 8 | Water | 341 | 3.98 |
| 29 | 545 | 2 | 195 | 10 | Water | 345 | 9.67 |
| 30 | 500 | 2 | 220 | 10 | Water | 156 | 10.76 |
| 31 | 500 | 2 | 220 | 10 | %25 polymer | 153 | 10.12 |
| 32 | 500 | 2 | 220 | 10 | %50 polymer | 150 | 10.28 |
| 33 | 500 | 2 | 220 | 10 | Air | 155 | 10.56 |

(*) AA6082-O was tested for comparison and validation.

## 2.2. Testing procedures for tensile strength, fatigue strength, impact resistance, and hardness

A Shimadzu Autograph 100 kN testing machine with a video type extensometer system was used to perform the tensile tests. The monotonic tension curve (strain $\varepsilon$ and stress $\sigma$) was constructed in the linear coordinate system by using specimens prepared following

the ASTM B557 M 02A standard [22] as seen in Fig. 2a. A 25 mm/min strain rate was applied for tensile tests for the aged specimens, while 1, 25, and 100 mm/min were used for determination of the strain rate sensitivity parameters in the jump test. Fig. 2b and c show the dimensions of the fatigue and impact test specimens prepared according to ASTM E606-92 [23] and ISO 148-1 [24] respectively. Fatigue tests were conducted at a constant frequency of 1 Hz, the load was fully reversed and the amplitude was kept constant to provide a zero mean stress. Since there is no endurance limit for nonferrous materials, the data was collected after 1 million cycles for AA6082.

(a)

(b)

(c)
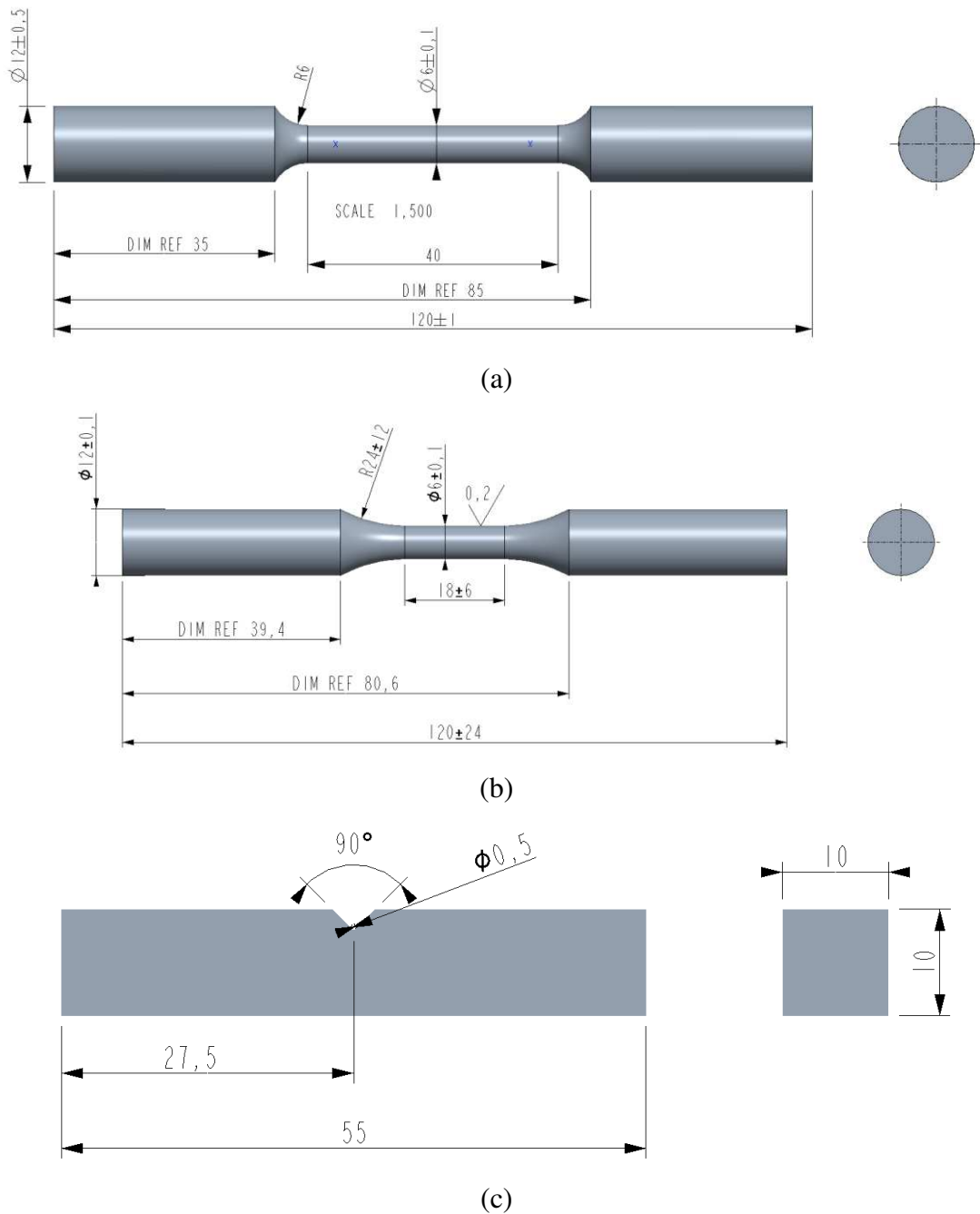
**Fig. 2** Dimensions of (a) tensile (b) fatigue (c) impact test specimens (mm)

Hardness measurements were carried out according to the ASTM E92 [25] standard by applying a 5 kg load for 15 seconds using the Vickers hardness measurement method. The hardness reading regions on the specimens are given in Fig. 3.
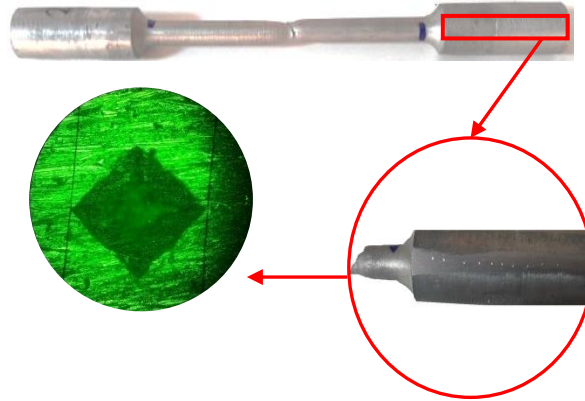


**Fig. 3** The measurement points for hardness

## 2.3. Microstructural investigation

For cold molding, the specimens were placed inside an epoxy filling material. They were grinded, polished, and etched, respectively. For these procedures, a Struers Labopol-5 automatic polishing unit was used. Sandpapers in the order of 320, 500, 1200, 2400, and 4000 grids were used successively for grinding. Specimens were cooled with pure water during the grinding process to prevent any microstructural change. Diamond suspensions in the different grain sizes and corresponding polishing fabrics were used in the polishing process. The finer grains lead to the less surface scratches. A uniform contact between the sample surface and the polishing fabric was confirmed during the polishing process in order to obtain a well-polished specimen surface. Various grain-sized polishing suspensions such as 3 μm, 1 μm, 0.25 μm and corresponding fabrics have been used. A fabric etchant was also used during the polishing to adjust the moisture content. Modified Keller's reagent (2.0 ml HF+98.0 ml $H_2O$) was used for etching during a 3 seconds soaking duration. An Olympus BX-51 optical microscope with X5-100 magnifications was used to take the microstructure images.

## 2.4. Hot forging experiment

A pair of a two-stage hot forging mold was used on a conventional screw press bench as seen in Fig. 4. The forging parameters such as press force, burr ratio, forging time, and mold filling rate were determined experimentally for various temperatures. The hot forging trials were carried out in the hot forging press workshop of DİTAŞ Inc. [26,27].
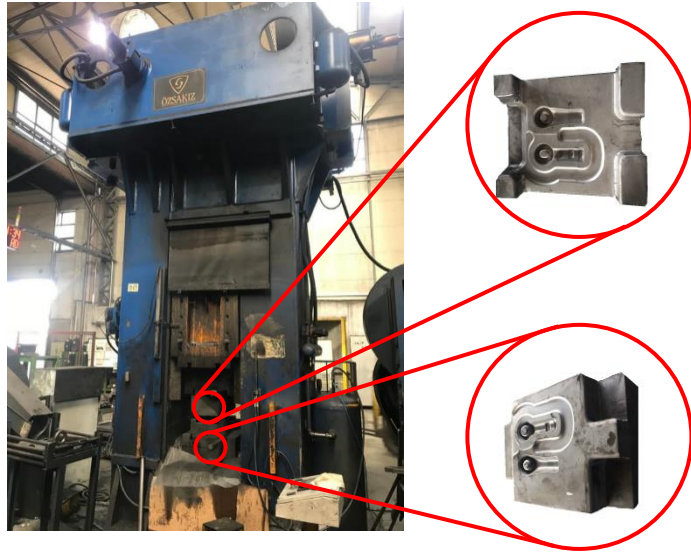


**Fig. 4** Hot forging press and tooling

## 2.5. Simulations

Finite element simulations of the hot forging and fatigue were performed. Fig. 5 shows a 3D finite element model, initial conditions, and mold-billet geometries for the forging simulations. The parameters such as press force, burr ratio, forging time, mold filling, and temperature were determined from the simulations for various temperatures. Deform © software [28] was used to perform hot forging simulations.
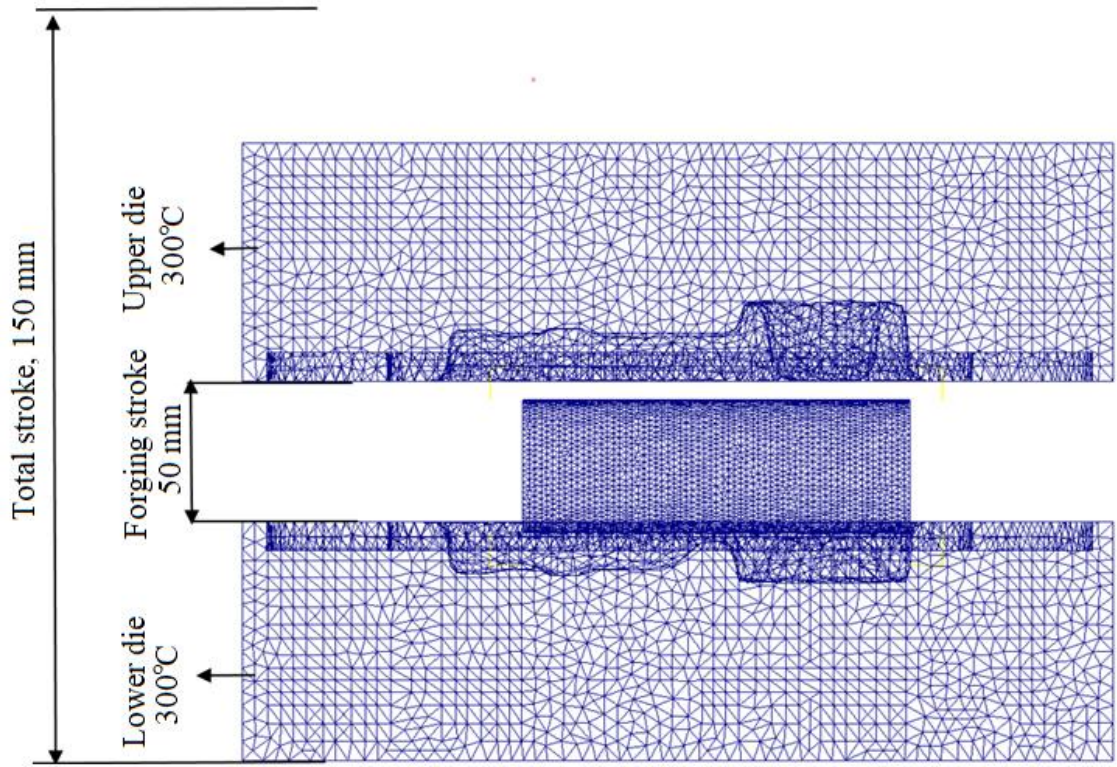
**Fig. 5** A finite element model of the hot forging process

The billet temperature was investigated between 300 - 525 °C for AA6082 and 750 - 1250 °C for AISI1045 steel for hot working conditions. Initial mold temperature was 300 °C for both materials. The simulations were repeated for 25 °C increments. Since the geometries were non-symmetric, the three dimensional (3D) model was used.

Tetrahedron elements were used for meshing and automatic re-meshing. 32670 elements were enough for converging in the results. The mesh of the outer surface of the mold was refined for getting accurate temperature distributions. The power function given in Eq. (1) [29] was employed as the isotropic hardening rule combined with the von Mises yield criterion [30] and associated flow rule to set the plasticity model for the cylindrical Ø25x100 mm billet material. The mold tools were set as rigid bodies.

$$\overline{\sigma} = c\,(\overline{\varepsilon})^n(\dot{\overline{\varepsilon}})^m + y \qquad\qquad \text{(Eq. 1)}$$

Here, $\overline{\sigma}$ is the equivalent stress, $\varepsilon$ is the plastic strain, $\overline{\varepsilon}$ is the equivalent plastic strain, $\dot{\overline{\varepsilon}}$ is the equivalent plastic strain rate. $y$, $c$, and $n$ are the yield point at the beginning, the strength coefficient, and the hardening exponent respectively. While $c$, $n$, and $y$ are

9

determined by curve fitting on the tensile curve, $m$ is the exponent of the strain rate sensitivity and determined from the jump test curve. The model's parameters were calculated from the curves of AA6082-O because the aged alloy turns into to AA6082-O at the hot forging temperature. The analysis time interval was set as 1 second and divided into 100 steps. The forging stroke is 50 mm. The upper mold moved linearly in the vertical direction while the lower mold was fixed. In order to avoid waste of time and unnecessary calculations, the upper mold was not retracted after forging. The analysis was performed explicitly. Direct solver has been chosen as a solver since it shortens the solution time. The coefficient of friction ($\mu$) was defined using the Coulomb friction model. The Coulomb friction coefficient at the tool and sample interface was assumed to be constant and taken as 0.3.

**Table 3** Material properties and model parameters

|  | AISI1045 | AA6082-O | AA6082 (*) |
|---|---|---|---|
| Density (gr/cm$^{3)}$ | 7.85 | 2.71 | 2.71 |
| Yield strength (**) (MPa) | 415.63 | 108.91 | 359.34 |
| Maximum strength (MPa) | 651.84 | 165.33 | 406 |
| Hardening exponent, $n$ | 0.369 | 0.613 | 0.347 |
| Strength coefficient, $C$ (MPa) | 730.421 | 220.207 | 189.759 |

(*) The specimen 18. (**) Proof strength for AA6082 alloy.

The fatigue simulations were carried out as the strength - life (S-N) type, with a fully reversed loading, and a constant amplitude which provides for a zero mean stress. The Soderbeg criterion was chosen as the mean stress correction theory, because of its conservative nature. Material properties in Table 3 for AA6082 and AISI1045 and experimental S-N data were used. Fatigue strength reduction factors $Kf$ = 0.634 for AA6082 and $Kf$ = 0.582 for AISI1045 [31] were used. The finite element model for fatigue analysis is given in Fig. 6. The 3D model was meshed with tetrahedron elements and the solution was performed in a one load step. Totally 1828757 elements were used for converging in the results.
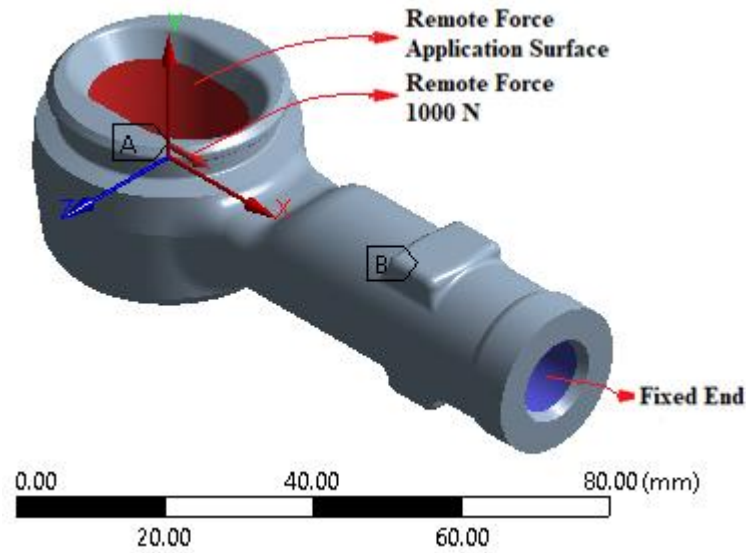
**Fig. 6** A finite element model for the fatigue simulation

## 3. RESULTS AND DISCUSSIONS

### 3.1. Mechanical properties

UTSs and strains at break for all samples are shown in Fig. 7a and b. The strains of the AA6082 samples were higher than the AISI1045 samples. It means that AA6082 has a higher formability than AISI1045. It is seen that the aging leads to a decrease in formability since the maximum strain is seen in AA6082-O, where artificial aging is not applied. Fig. 7a indicates that UTSs of AA6082 samples were much lower than the AISI1045 sample, which was about 711 MPa. The highest value of AA6082 was 406 MPa.
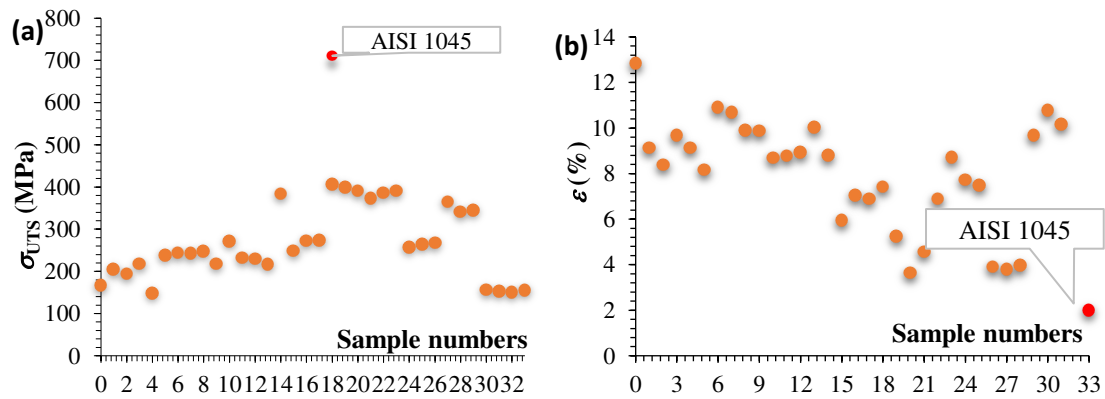


**Fig. 7** (a) UTSs and (b) strains at break of the AA6082 samples

11

Engineering stress vs. strain curves of the materials are given in Fig. 8. Although the strength of the AA6082-O samples was quite low, the aged AA6082 sample was improved significantly in strength. It has also higher formability inherently. Yield points of the samples were noticeably distinctive.
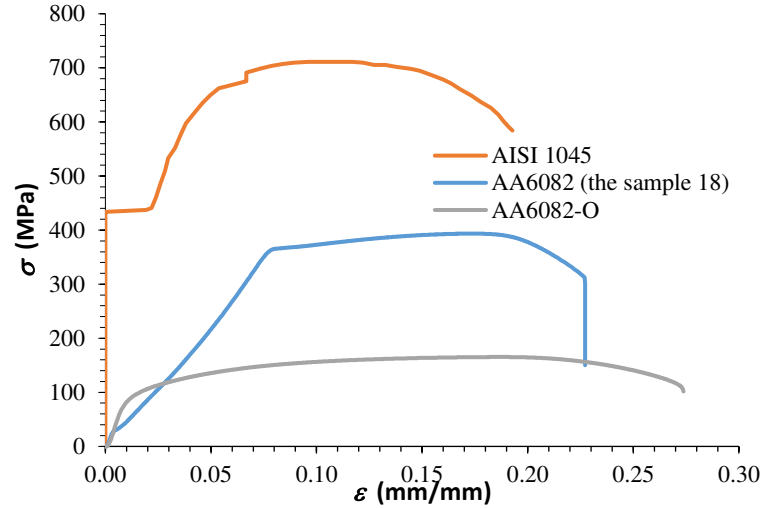


**Fig. 8** Comparison of engineering tensile curves of AA6082 and AISI1045

Hardness and the Charpy impact tests were also conducted as seen in Fig. 9. It is clear that the hardness of AA6082 increases after all aging treatments. Increased hardness provides more wear resistance but suffers from the toughness. However, the energy-absorbing capability of AA6082 is higher than that of AISI1045. It is also noticed that the hardness decreases from 175 HV to 122 HV when AA6082 was pre-strained. Some researchers have shown that the hardness of aluminum-based alloys has decreased with pre-strain [32-36]. However, steel-based materials have opposite attitude [37-39].
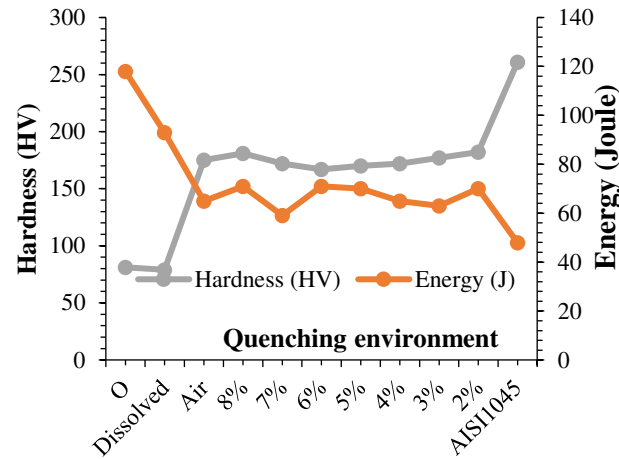
**Fig. 9** Hardness and Charpy impact energy

The Wöhler curves were drawn as shown in Fig. 10. While the endurance limit of AISI1045 was 300 MPa, the fatigue strength of AA6082 for more than a million cycles was obtained for the specimen 18 with laboratory-controlled fatigue tests. It is clearly seen no infinite life in AA6082. This is very well-known issue in aluminum alloys.
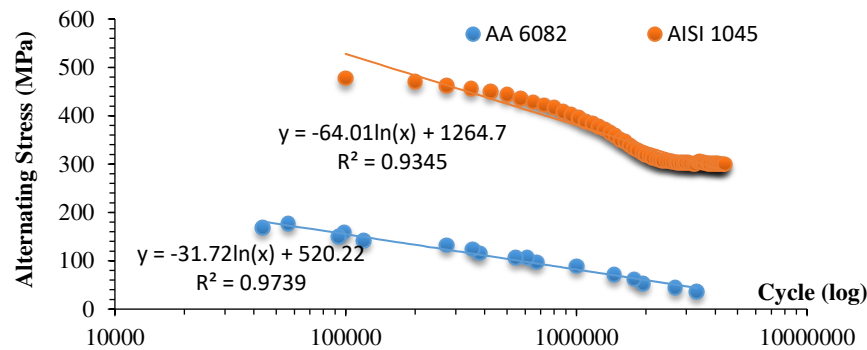


**Fig. 10** Wöhler curves of AISI1045 and the specimen 18

## 3.2 Jump test

The strain rate sensitivity coefficient "*m*" to be used in the plasticity equation in the simulations was calculated by using the jump test. The jump test was performed at the room temperature in the tensile test with 1 and 100 mm/min strain rates. A curve was conducted as seen in Fig. 11. The figure also includes the calculation method. The curve

includes just true plastic data. Removing the elastic strain was explained in [40] in detail.
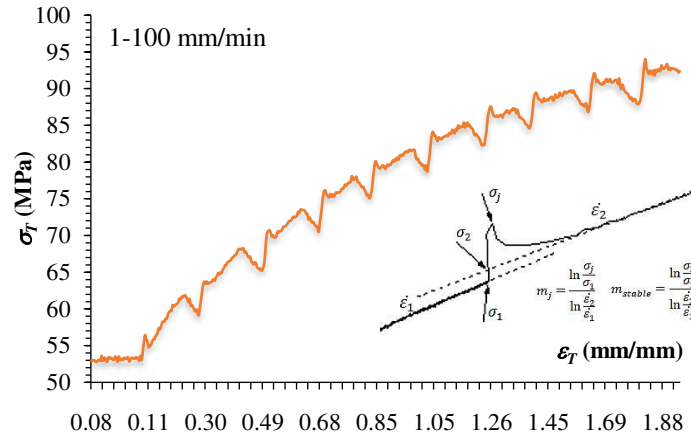


**Fig. 11** Jump test curve

The results are seen in Table 4 where $\dot{\varepsilon}_1$ and $\dot{\varepsilon}_2$ are the strain rates before and after a peak respectively. While $\sigma_1$ stands for the stress at the beginning of the peak, $\sigma_j$ is the stress at the peak point. $\sigma_2$ is the stress at the intersection point of the peak.

**Table 4** Calculations from the jump peaks

| No. | $\sigma_1$ (MPa) | $\sigma_j$ (MPa) | $\dot{\varepsilon}_1$ (mm/min) | $\dot{\varepsilon}_2$ (mm/min) | $m_j = \left(\ln\dfrac{\sigma_j}{\sigma_1}\right) / \left(\ln\dfrac{\dot{\varepsilon}_2}{\dot{\varepsilon}_1}\right)$ |
|---|---|---|---|---|---|
| 1 | 53.040 | 54.860 | 0.090 | 0.100 | 0.320 |
| 2 | 59.160 | 60.430 | 0.300 | 0.310 | 0.648 |
| 3 | 65.380 | 70.430 | 0.480 | 0.550 | 0.547 |
| 4 | 70.520 | 71.060 | 0.680 | 0.690 | 0.523 |
| 5 | 75.090 | 76.140 | 0.850 | 0.870 | 0.597 |
| 6 | 78.680 | 80.125 | 1.040 | 1.070 | 0.640 |

### 3.3 Microstructure evaluation

AA6082 basically contains the elements Al, Mg, Si, Ti, Cr, Mn, Fe, Cu, and Zn. The most common intermetallic phase is $Mg_2S$. This phase appears as dark regions in the microstructure images. Fe and Mn elements lead to very small amounts of impurities. Fe and Al form double, triple, and quadruple intermetallic phases such as Al-Fe, Al-Fe-Si and Al-Fe-Mn-Si. Mn and Cr are elements which balance the Fe content in $\alpha$-$Al_{12}(FeMn)_3Si$ or $\alpha$-$Al_{12}$ $(FeCr)3Si$. The $\alpha$ phases are detrimental to the mechanical properties. $\beta$-$Al_9Fe_2Si_2$ or $\beta$-$Al_5FeSi$ phases contain Fe and Si in the dendritic shape.

Intermetallic phases settle in the grain boundary. Microstructure photographs are shown in Fig. 12 where O: Al, □: Mg$_2$Si, Δ:α-dendrite, ⬭: β-dendrite.

**Fig. 12** Optic examinations **a** AA6082-O **b** water quenching, 2 h aging at 175°C **c** water quenching, 4 h aging at 175°C **d** water quenching, 8 h aging at 175°C **e** water quenching, 10 h aging at 175°C **f** water+50%polymer mix quenching, 10 h aging at 175°C **h** water quenching, 2 h aging at 185°C **i** water quenching, 4 h aging at 185°C **j** water quenching, 6 h aging at 185°C **k** water quenching, 8 h aging at 185°C **l** water quenching, 10 h aging at 185°C **m** water+50%polymer mix quenching, 10 h aging at 185°C **n:** water quenching, 2 h aging at 195°C **o** water quenching, 4 h aging at 195°C **p** water quenching, 6 h aging at 195°C **q** water quenching, 8 h aging at 195°C **r** water quenching, 10 h aging at 195°C **s** water+50%polymer mix quenching, 6 h aging at 195°C **t** water+50%polymer mix quenching, 2 h aging at 175°C **u** water+50%polymer mix quenching , 4 h aging at 185°C **v:** water+50%polymer mix quenching, 6 h aging at 195°C **y:** water+50%polymer mix quenching, 10h aging at 220°C.

Lighter-colored regions in the microstructure images show essential Al elements. As the temperature and artificial aging time increase, the grain size decreases. The amount and size of the dendrites increase with increasing aging time. Smaller and homogeneous precipitate distribution was obtained by quenching in the 50% polymer + water mixture.

It is observed that the coarse grains were completely dissolved in the microstructure for the samples aged at 175 °C. The $\beta$-dendrites have a longer and thicker shape as reported [15,16]. The micro impurities settled in the grain boundaries lead to an easier movement of the dislocations during deformation. This provides ductility.
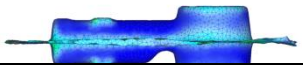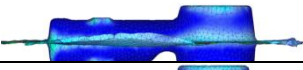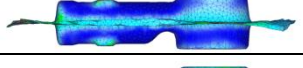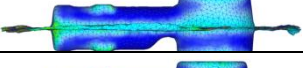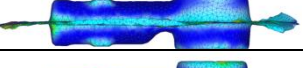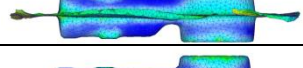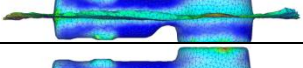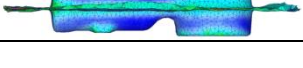
When the samples aged at 185 °C were compared to the ones aged at 175 °C, it is seen that the grain size was smaller, which is especially noticeable when the aging time

16

increases. The shape of the Mg₂Si precipitates becomes smaller and its amount increases. In addition, $\alpha$-dendrites and $\beta$-dendrites at 185 °C were smaller than those at 175 °C and stayed in the needle-like shapes. The highest UTS was obtained from the sample aged at 185 °C for 4 hours. The grains were dissolved in a smaller distribution in samples aged at 195 °C. As the aging time increases, the grain sizes decrease. The Mg₂Si phases became smaller and its amount increases. Although the $\alpha$-dendrites and $\beta$-dendrites, which are in a needle-like shape, were visible at 185 °C, they became smaller and disappeared in the microstructure at 195 °C. Since the $\beta''$-(Mg5Si6) phase seen up to 300 °C [17], both phases were not seen between 175-220°C.

## 3.4 Hot forging

It is seen that the pressing force requirement decreased at elevated initial billet temperature due to the decreasing yield point. Tables 5 and 6 compare the forging results for AA6082 and AISI1045, respectively.

**Table 5** Hot forging simulation results of AISI1045

| Initial temp. (°C) | Peak temp. (°C) | Press force (tons) | Mold filling | Burr (%) |
|---|---|---|---|---|
| 750 | 1320 | 1770 |  | 5.37 |
| 775 | 1340 | 1940 |  | 5.54 |
| 800 | 1350 | 1700 |  | 5.55 |
| 825 | 1330 | 1540 |  | 5.47 |
| 850 | 1320 | 1770 |  | 5.49 |
| 875 | 1310 | 1630 |  | 5.52 |
| 900 | 1330 | 1580 |  | 5.55 |
| 925 | 1350 | 1560 |  | 5.55 |
| 950 | 1330 | 1550 |  | 5.64 |
| 975 | 1320 | 1500 |  | 5.52 |
| 1000 | 1340 | 1400 |  | 5.60 |

| | | | | |
|---|---|---|---|---|
| 1025 | 1350 | 1090 | | 5.55 |
| 1050 | 1290 | 872 | | 5.37 |
| 1075 | 1290 | 1010 | | 5.49 |
| 1100 | 1290 | 902 | | 5.64 |
| 1125 | 1280 | 876 | | 5.4 |
| 1150 | 1360 | 1000 | | 5.47 |
| 1175 | 1330 | 715 | | 5.40 |
| 1200 | 1350 | 727 | | 5.64 |
| 1225 | 1370 | 801 | | 5.55 |
| 1250 | 1360 | 715 | | 5.52 |
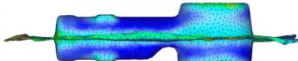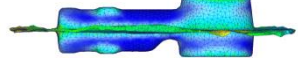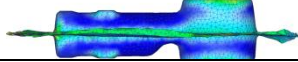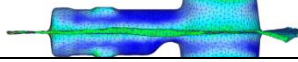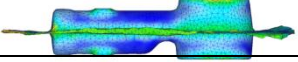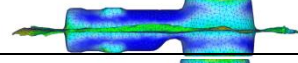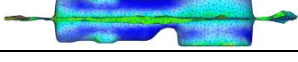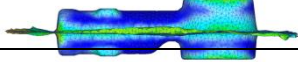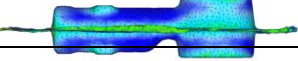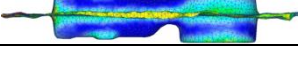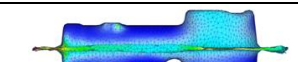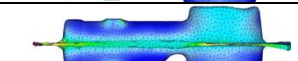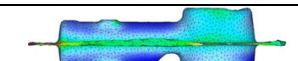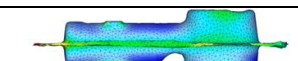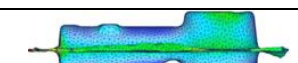
**Table 6** Hot forging simulation results of AA6082

| Initial temp. (°C) | Peak temp. (°C) | Press force (tons) | Mold filling | Burr (%) |
|---|---|---|---|---|
| 300 | 648 | 413 | | 3.75 |
| 325 | 639 | 437 | | 4.13 |
| 350 | 660 | 397 | | 4.11 |
| 375 | 577 | 311 | | 4.15 |
| 400 | 651 | 353 | | 4.12 |
| 425 | 516 | 155 | | 5.11 |
| 450 | 651 | 353 | | 5.17 |
| 475 | 516 | 153 | | 4.93 |
| 500 | 561 | 145 | | 4.97 |
| 525 | 581 | 140 | | 5.07 |

The forging increases the strain energy and billet temperature, as expected. The temperature variation in the steel was relatively smaller than AA6082. When the initial

temperature of the AA6082 billet exceeded 450 °C, the body temperature might reach up to the melting point locally. Melted material cannot fill the mold cavity properly and also leads to more burr formation. The temperature change seen during hot forging was more stable for AISI1045. It is concluded that the initial billet temperature must be less than 450 °C.

The forged AA6082 rod ends at elevated temperatures are given in Fig. 13 for comparison and validation. The amount of burr, the surface condition, and the mold filling ratio can be seen from the figure. The mold cavity was not completely filled during forging at higher temperatures than 400 °C. Thus, the amount of burr increased, which confirmed the simulation predictions.
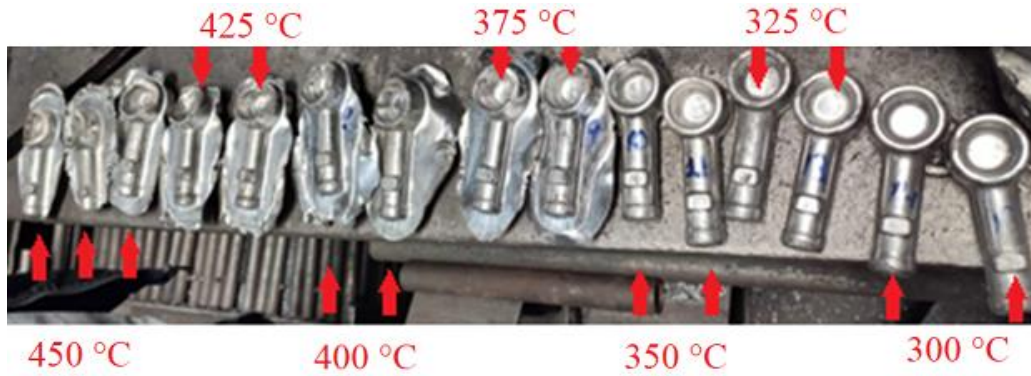


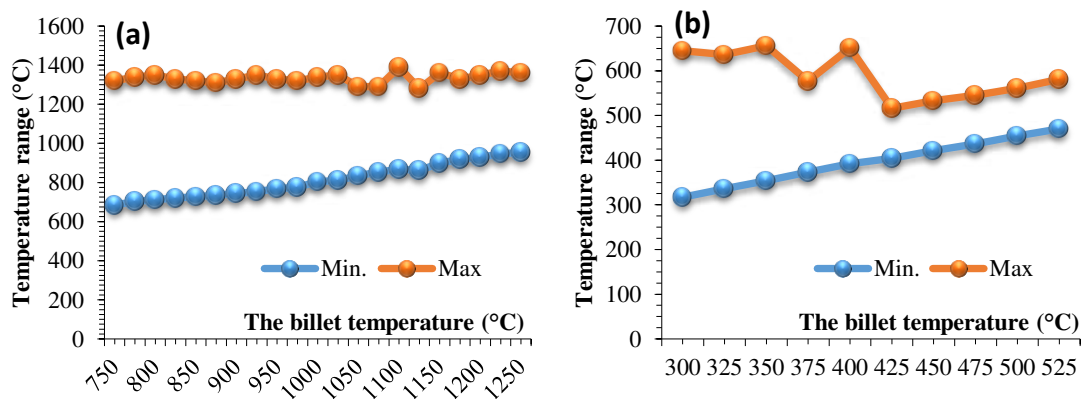**Fig. 13** The hot forging of the rod end at elevated temperatures



**Fig. 14** The billet temperature ranges during the hot forging of (*a*) AISI1045 and (*b*) AA6082

As seen in Fig. 14, the billet temperature increased during forging due to increasing strain energy. While the maximum temperature was stable and stayed under the melting

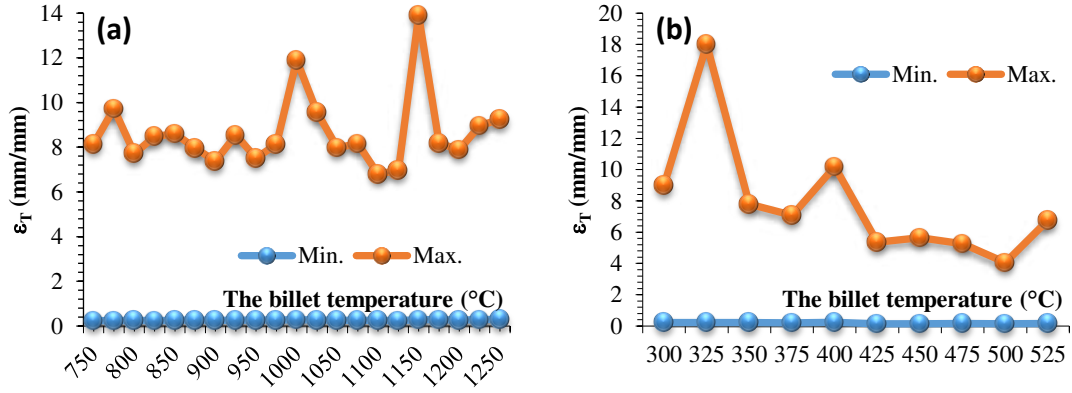point for the steel, it may excess the melting point for AA6082 causes incomplete mold filling.



**Fig. 15** The strain in the hot forging of (*a*) AISI1045 and (*b*) AA6082

Fig. 15 shows that the deformation of AA6082 alloy was more temperature dependent. While AA6082 alloy has the highest forgeability at 325 °C, it was 1150 °C for the steel. The fact that the deformation capability was decreased for AA6082 as the temperature increases caused incomplete mold cavity due to the liquid flow of the melted material. Considering the difference in the temperature and the specific heat capacity, which is 950 J/kg.°K for aluminum and 480 J/kg.°K for steels [41], a 39.01% saving in energy per part can be achieved by replacing with AA6082.
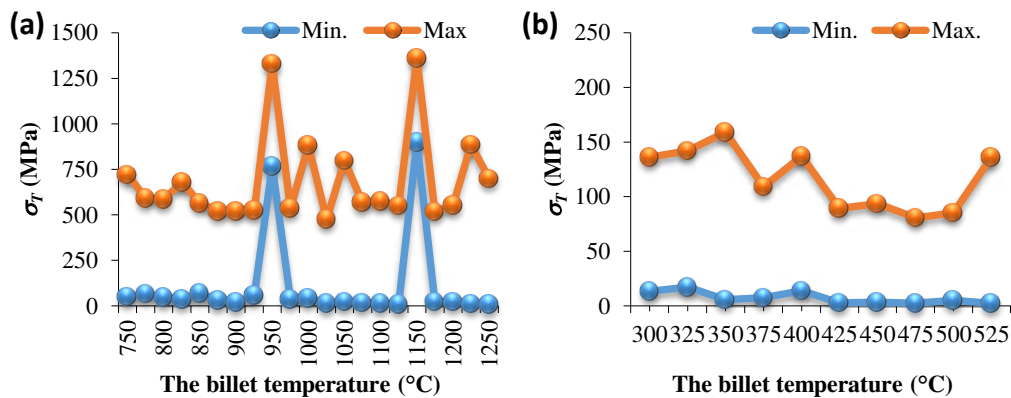


**Fig. 16** The stress in the hot forging of (*a*) AISI1045 and (*b*) AA6082

As seen in Fig. 16, the residual stress remained in the forged part was lower in AA6082. It means that the part to be produced from aluminum alloy does not need an additional heat treatment for stress relief after the hot forging. The press force required for hot

20

forging of AA6082 alloy was also less as seen in Fig. 17. This affects the competitiveness of the rod end manufacturers by reducing the operating and manufacturing costs.
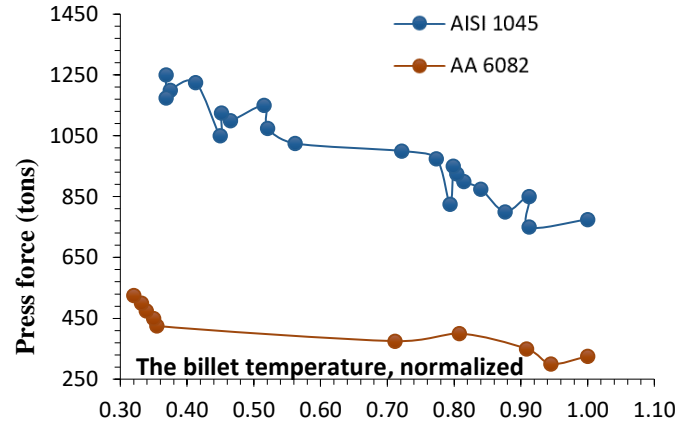


**Fig. 17** Press force requirements

## 3.5 Fatigue simulation

Fig. 18 shows the safety factor, yield stress, service life, and the biaxial stress distribution results of the rod end loaded to service conditions. As can be deducted from the safety factor solutions, the thinner section was the most sensitive to fatigue. The lowest safety factor was 5.34 for AISI1045, while it was 1.94 for the AA6082 sample 18. The entire part has a sufficient fatigue and static stress capacity for infinite life. Thus the replacement of AISI1045 with AA6082 is possible without sacrificing the fatigue requirements.
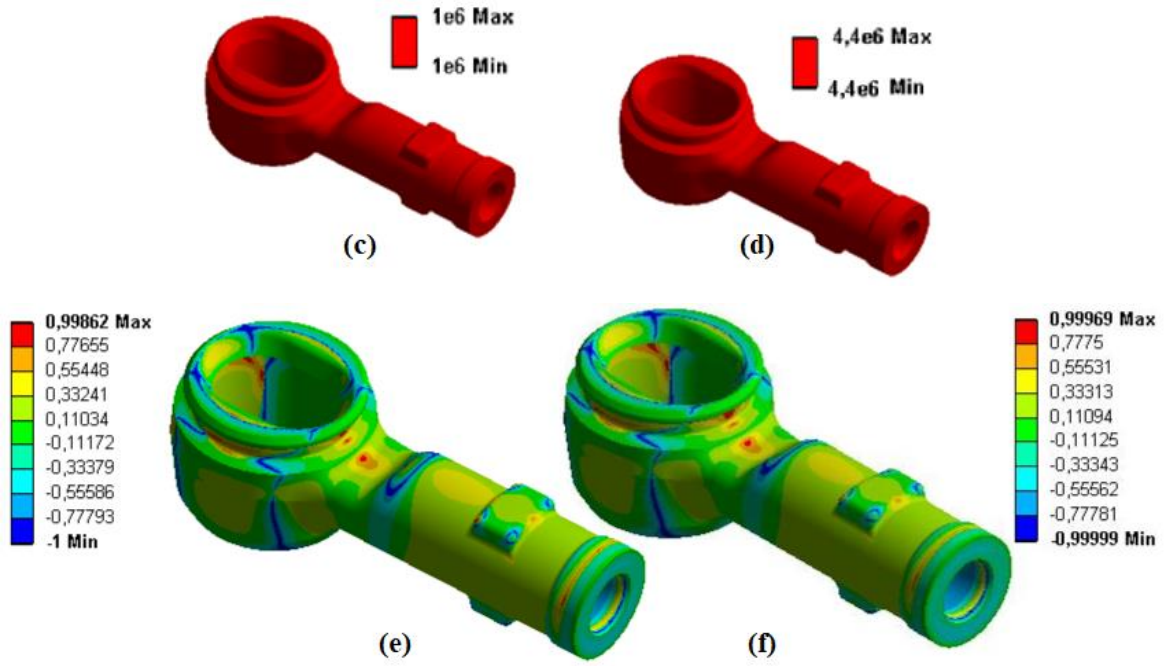


21
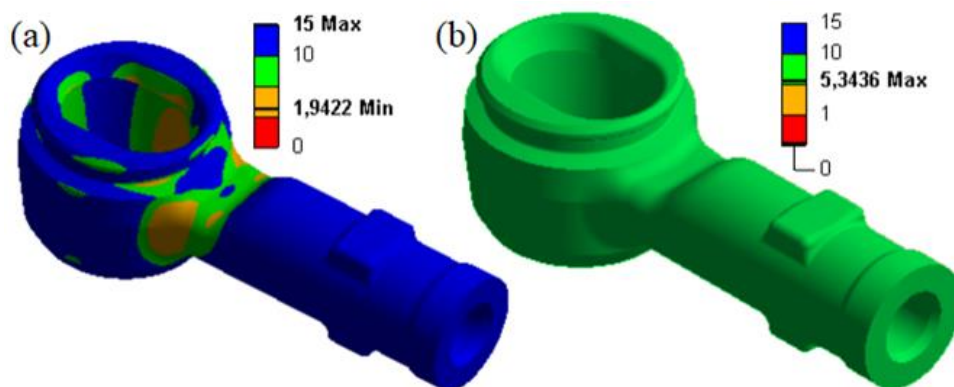
**Fig. 18** Safety factor solutions (a) for AA6082 (b) for AISI1045. Service life (c) for AA6082 (d) for AISI1045. Biaxial stress solution (e) for AA6082 (f) for AISI1045

From the biaxial stress solution, it can be seen that normal and shear stresses were present at the body surface. Equivalent von Mises stress distribution is given in Fig. 19. While the maximum equivalent stress was 41.264 MPa for AISI1045, it was 44.38 MPa for AA6082.
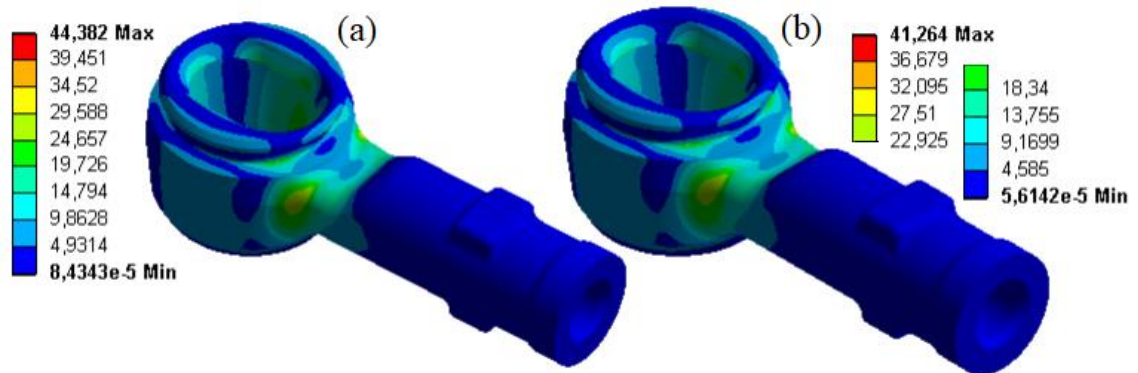


**Fig. 19** Stress solutions (MPa) (a) for AA6082 (b) for AISI1045

For a manufacturer in the competitive world, it is quite important to replace a structural part with the lighter one without sacrificing safety, manufacturing time, and low cost. It

is a challenge to replace the material of the forged rod end part. So all vehicles having the transmission will be lightened.

Summarizing the whole results above, the most important contributions of this study are that the aged AA6082 sample was improved significantly in strength as explained by Kvackaj et al. (2009) [2]. $\beta$ phases playing important role in the strengthening have a finer distribution in the microstructure up to 4 hours of aging [17]. The optimum forging temperature is between 300 - 450 °C which is lower than that of AISI1045 [10]. Increased hardness provides more wear resistance. The fatigue life is more than a million cycles with 1.94 safety factor which is higher than 1.5, as a rule of thumb [31]. The increased hardness and the fatigue life increase the damage tolerance like Al-Li based alloys [42] which are another material used in the aerospace and automotive industry. Thus, AA6082 would be a good replacement for applications where shock and vibrational loads are to be expected due to the higher energy-absorption capability.

In this study, the mechanical test was performed to identify plasticity model parameters and the processes were simulated. The strengthening and hardening behavior were exposed by microstructural investigations. For the validation, hot forging experiments were performed. Results proved that the artificially aged AA6082 could be used for a replacement of the AISI1045 rod end without changing the part design and the manufacturing process. The critical point is that the lower temperature requirement leads to the more economical forging process. Hence, it becomes a cheaper alternative among other aluminum alloys. So it makes the alloy most important for the forged part manufacturers.

## 4. CONCLUSIONS

In this study, a possible replacement of AISI1045 with AA6082 was investigated for an automotive structural part. The most suitable artificial aging conditions were determined for AA6082. The results were used in the fatigue and hot forging simulations. Microstructural analysis was also performed. The fatigue life of the rod end, the press force requirement for the forging process, the burr ratio and the processing time have been evaluated. The most important conclusions can be summarized as follows;

- The highest tensile strength of 406 MPa can be achieved by dissolving at 500 °C for 2 hours, quenching in air, aging at 185 °C for 4 hours, and cooling in air. Under these circumstances, the AA6082 rod end has at least one million cycles service life. Although increased hardness provides more wear resistance to AA6082, it suffers from energy-absorbing capability.

- Aged alloy's cold forgeability is poor due to brittle nature of the material and crack initiations. Thus warm or hot forging is recommended.

- For warm forging of the alloy, it is recommended to maintain temperature ranges of 160 - 300 °C for a good microstructure, strength, and forging-energy absorption capability.

- For hot forging of the alloy, more than 425 °C billet temperature is not suitable. Because the local material melting during process causes incomplete mold filling. It is concluded that the hot forging up to 425 °C is suitable.

- AA6082 would be a good replacement for applications where shock and vibrational loads are to be expected due to the higher energy-absorbing capability.

- $\beta$ phases are the most effective for strengthening of AA6082. $\beta$ phases have a finer distribution in the microstructure up to 4 hours of aging. Longer aging time results in coarser grains, dendrite formation, and reduced strength.

- AA6082 can lead to less energy consumption during manufacturing and guarantees more economical manufacturing without sacrificing service requirements. The rod end part currently manufactured from AISI1045 can be replaced by AA6082 without any design changes.

**ACKNOWLEDGEMENTS**

## Compliance with ethical standards

**Conflict of interest** The authors declare that they have no conflicts of interest.

**Ethical approval** n/a

**Consent to participate** n/a

**Consent to publish** Yes

## REFERENCES

1. Zvinys J, Kandrotaite Janutiene R, Meskys J, Juzenas K (2012) Investigation of thermo mechanical effect on structure and properties of aluminium alloy 6082. Int Virtual J Sci Tech Innov Ind:3-6
2. Kvackaj T, Fujda M, Besterci M (2009) Ultra Fine Microstructure and Properties Formation of EN AW 6082 Alloy. Transactions of the Japan Society for Aeronautical and Space Sciences, Space Technology Japan 7 (ists26):Pc_85-Pc_91. doi:10.2322/tstj.7.Pc_85
3. Prabhukhot A (2015) Effect of Heat Treatment on Hardness and Corrosion Behavior of 6082-T6 Aluminium Alloy in Artificial Sea Water. International Journal of Materials Science and Engineering 3:287-294. doi:10.17706/ijmse.2015.3.4.287-294
4. Torca I, Aginagalde A, Esnaola JA, Galdos L, Azpilgain Z, Garcia C (2010) Tensile Behaviour of 6082 Aluminium Alloy Sheet under Different Conditions of Heat Treatment, Temperature and Strain Rate. Key Engineering Materials 423:105-112. doi:10.4028/www.scientific.net/KEM.423.105
5. Bouquerel J, Diawara B, Dubois A, Dubar M, Vogt JB, Najjar D (2015) Investigations of the microstructural response to a cold forging process of the 6082-T6 alloy. Mater Design 68:245-258. doi:https://doi.org/10.1016/j.matdes.2014.12.005

6. Chang Y-L, Hung F-Y, Lui T-S (2019) Study of microstructure and tensile properties of infrared-heat-treated cast-forged 6082 aluminum alloy. Journal of Materials Research and Technology 8 (1):173-179. doi:https://doi.org/10.1016/j.jmrt.2017.10.004

7. Krolo J, Lela B, Ljumović P, Bagavac P (2019) Enhanced Mechanical Properties of Aluminium Alloy EN AW 6082 Recycled without Remelting. Tehnicki Vjesnik 26:1253-1259. doi:10.17559/TV-20180212160950

8. Kumar N, Jayaganthan R, Brokmeier H-G (2017) Effect of deformation temperature on precipitation, microstructural evolution, mechanical and corrosion behavior of 6082 Al alloy. T Nonferr Metal Soc 27 (3):475-492. doi:https://doi.org/10.1016/S1003-6326(17)60055-4

9. Gökçil E, Akdi S, Birol Y (2015) A novel processing route for the manufacture of EN AW 6082 forged components. Mater Res Innov 19:S10-311. doi:10.1179/1432891715Z.0000000002179

10. Birol Y, Ilgaz O, Akdi S, Unuvar E (2014) Comparison of Cast and Extruded Stock for the Forging of AA6082 Alloy Suspension Parts. Advanced Materials Research 939:299-304. doi:10.4028/www.scientific.net/AMR.939.299

11. Birol Y, Gökçil E, Akdi S (2017) Potential of twin-belt-cast EN AW 6082 blanks for the manufacture of wishbone suspension forgings. Int J Adv Manuf Technol 92. doi:10.1007/s00170-017-0446-3

12. Kumar N, Goel S, Rengaswamy J, Brokmeier H-G (2015) Effect of Solution Treatment on Mechanical and Corrosion Behaviors of 6082-T6 Al Alloy. Metallography, Microstructure and Analysis 4:411-422. doi:10.1007/s13632-015-0219-z

13. Shao Z, Lee J, Wang J, Lin J, Jiang J (2020) A study of various heating effects on the microstructure and mechanical properties of AA6082 using EBSD and CPFE. J Alloy Compd 818:152921. doi:https://doi.org/10.1016/j.jallcom.2019.152921

14. Sürmen Ö, Tarakçı M, Gencer Y, Zeytin S Improvement of Heat Treatment Application of Aluminium Forged Parts. In: IMMC 2016, 18th International Metallurgy & Materials Congress, 2016. UCTEA Chamber of Metallurgical & Materials Engineers, pp 721-724

15. Mrówka-Nowotnik G, Sieniawski J (2005) Influence of heat treatment on the microstructure and mechanical properties of 6005 and 6082 aluminium alloys. Journal of Materials Processing Technology 162-163:367-372. doi:https://doi.org/10.1016/j.jmatprotec.2005.02.115

16. Österreicher J, Kumar M, Schiffl A, Schwarz S, Hillebrand D, Bourret G (2016) Sample preparation methods for scanning electron microscopy of homogenized Al-Mg-Si billets: A comparative study. Mater Charact 122. doi:10.1016/j.matchar.2016.10.020

17. Yibo P, Gang W, Tianxing Z, Shangfeng P, Yiming R (2013) Dynamic Mechanical Behaviors of 6082-T6 Aluminum Alloy. Adv Mech Eng 5:878016. doi:10.1155/2013/878016

18. Kumar M, Baloch M, Abro MI, Memon S, Chandio A (2019) Effect of Artificial Aging Temperature on Mechanical Properties of 6061 Aluminum Alloy. Mehran University Research Journal of Engineering and Technology 38:31-36. doi:10.22581/muet1982.1901.03

19. Xu Z, Ma H, Zhao N, Hu Z (2020) Investigation on Compressive Formability and Microstructure Evolution of 6082-T6 Aluminum Alloy. Metals-Basel 10:469. doi:10.3390/met10040469

20. Cabibbo M, Evangelista E, Vedani M (2005) Influence of severe plastic deformations on secondary phase precipitation in a 6082 Al-Mg-Si alloy. Metallurgical

and Materials Transactions A: Physical Metallurgy and Materials Science 36:1353-1364. doi:10.1007/s11661-005-0226-9

21. Ben Naser T, Bobor K, Krallics G (2014) Tensile behavior of multiple forged 6082 Al alloy. Periodica Polytechnica Mechanical Engineering 58. doi:10.3311/PPme.7275

22. ASTM (2002) Standard Test Methods of Tension Testing Wrought and Cast Aluminum- and Magnesium-Alloy Products. vol ASTM B 557M – 02a. ASTM International, West Conshohocken, PA 19428-2959, United States

23. ASTM (2004) Standard Practice for Strain-Controlled Fatigue Testing. vol ASTM E 606 – 92. ASTM International, West Conshohocken, PA 19428-2959, United States

24. ISO (2016) Metallic materials — Charpy pendulum impact test — Part 1: Test method. vol ISO 148-1:2016. International Organization for Standardization, Geneva, Switzerland

25. ASTM (2017) Standard Test Methods for Vickers Hardness and Knoop Hardness of Metallic Materials. vol ASTM E 92. ASTM International, West Conshohocken, PA 19428-2959, United States

26. Inc. D (2020) Hot forging press workshop Ditas Academia

27. Tunc O (2020) Investigation on forging performance of AA6082. MSc., Nigde Omer Halisdemir University, Niğde

28. SFTC (2020) DEFORM V12.0.2 User's Manual. Scientific Forming Technologies Corporation, Columbus, Ohio

29. Ludwik P (1909) Elemente der Technologischen Mechanik. Springer-Verlag Berlin Heidelberg. doi:10.1007/978-3-662-40293-1

30. Mises RV (1928) Mechanik der plastischen Formänderung von Kristallen. ZAMM - Journal of Applied Mathematics and Mechanics / Zeitschrift für Angewandte Mathematik und Mechanik 8 (3):161-185. doi:10.1002/zamm.19280080302

31. Budynas R, Nisbett K (2010) Shigley's Mechanical Engineering Design. McGraw-Hill Education,

32. Al-Rubaie KS, Del Grande MA, Travessa DN, Cardoso KR (2007) Effect of pre-strain on the fatigue life of 7050-T7451 aluminium alloy. Materials Science and Engineering: A 464 (1):141-150. doi:https://doi.org/10.1016/j.msea.2007.02.024

33. Kilic S, Kacar I, Sahin M, Ozturk F, Erdem O (2019) Effects of Aging Temperature, Time, and Pre-Strain on Mechanical Properties of AA7075. Materials Research 22

34. Thangarasu A, Murugan N, Dinaharan I (2014) Production and Wear Characterization of AA6082 -TiC Surface Composites by Friction Stir Processing. Procedia Engineering 97:590-597. doi:https://doi.org/10.1016/j.proeng.2014.12.287

35. Werber A, Liewald M (2012) Influence of pre-strain and heat treatment on mechanical properties of aluminum sheet. Int J Mater Form 5 (4):307-315. doi:10.1007/s12289-011-1051-x

36. Ozturk F, Toros S, Kilic S (2010) Tensile deformation behavior of AA5083-H111 at cold and warm temperatures. Int J Mater Res 101 (9):1172-1179. doi:10.3139/146.110391

37. Kılıç S (2016) Twip Çeliklerde İkizlenme Mekanizmasının Mekanik Özelliklere Etkisinin İncelenmesi. Niğde University, Niğde

38. Kilic S, Ozturk F, Picu CR (2018) Investigation of the Performance of Flow Models for TWIP Steel. J Mater Eng Perform 27 (8):4364-4371. doi:10.1007/s11665-018-3504-6

39. Zulfi FR, Korda AA (2016) Effect of pre-strain on mechanical properties and deformation induced transformation of 304 stainless steel. Journal of Physics: Conference Series 739:012039. doi:10.1088/1742-6596/739/1/012039

40. Kacar İ, Kılıç S (2018) Hardening rules. In: Güngör PDT, Kılıç DDGB, Uyumaz DDA, Görgülü DÖÜS (eds) Innovative Approaches in Engineering. Gece Kitaplığı, ANKARA / TURKEY, pp 175-194

41. Çengel YA (1998) Heat Transfer: A Practical Approach. WBC McGraw-Hill,

42. Kilic S, Kacar I, Ozturk F (2019) New trend in aerospace industry: Al-Li based alloys. J Fac Eng Archit Gaz 34 (1):275-296
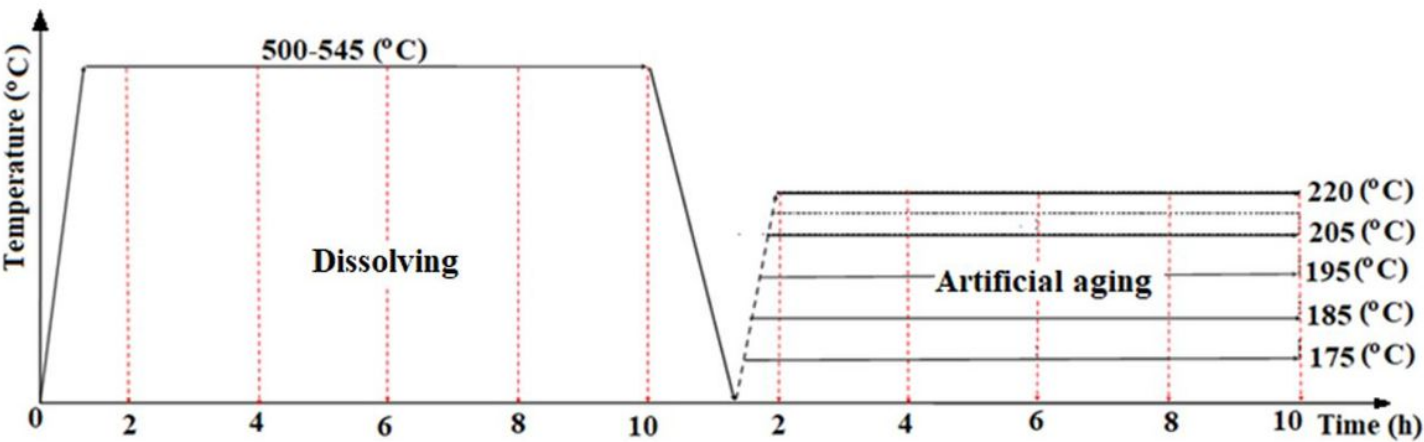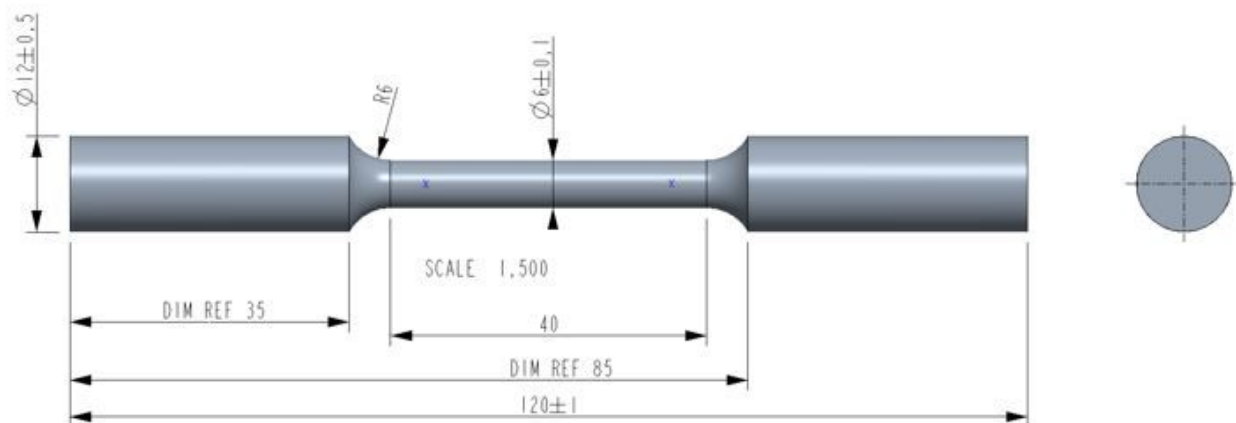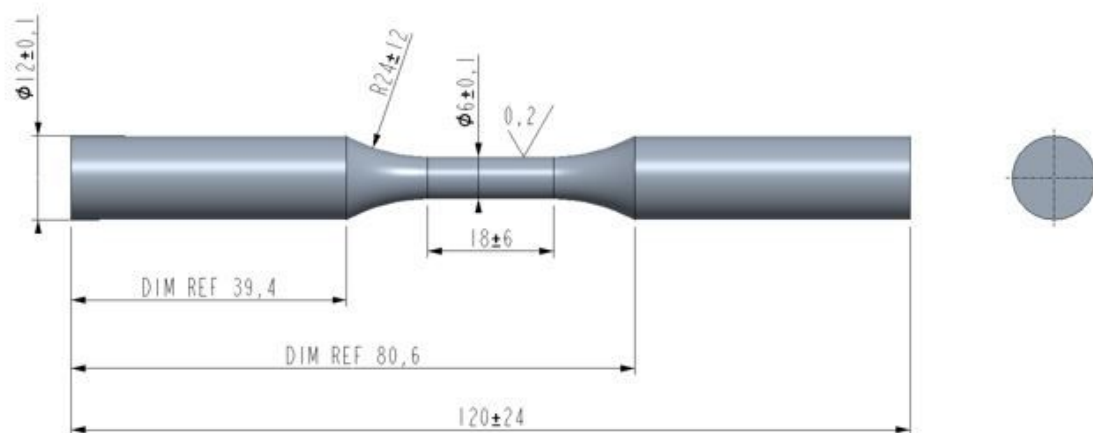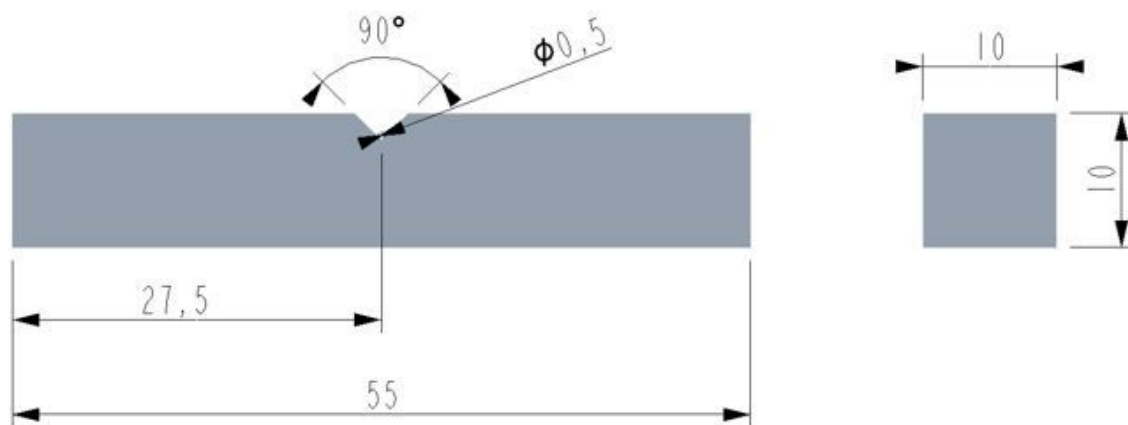
# Figures



**Figure 1**

A scheme for the heat treatment cycle

Figure 2

Dimensions of (a) tensile (b) fatigue (c) impact test specimens (mm)
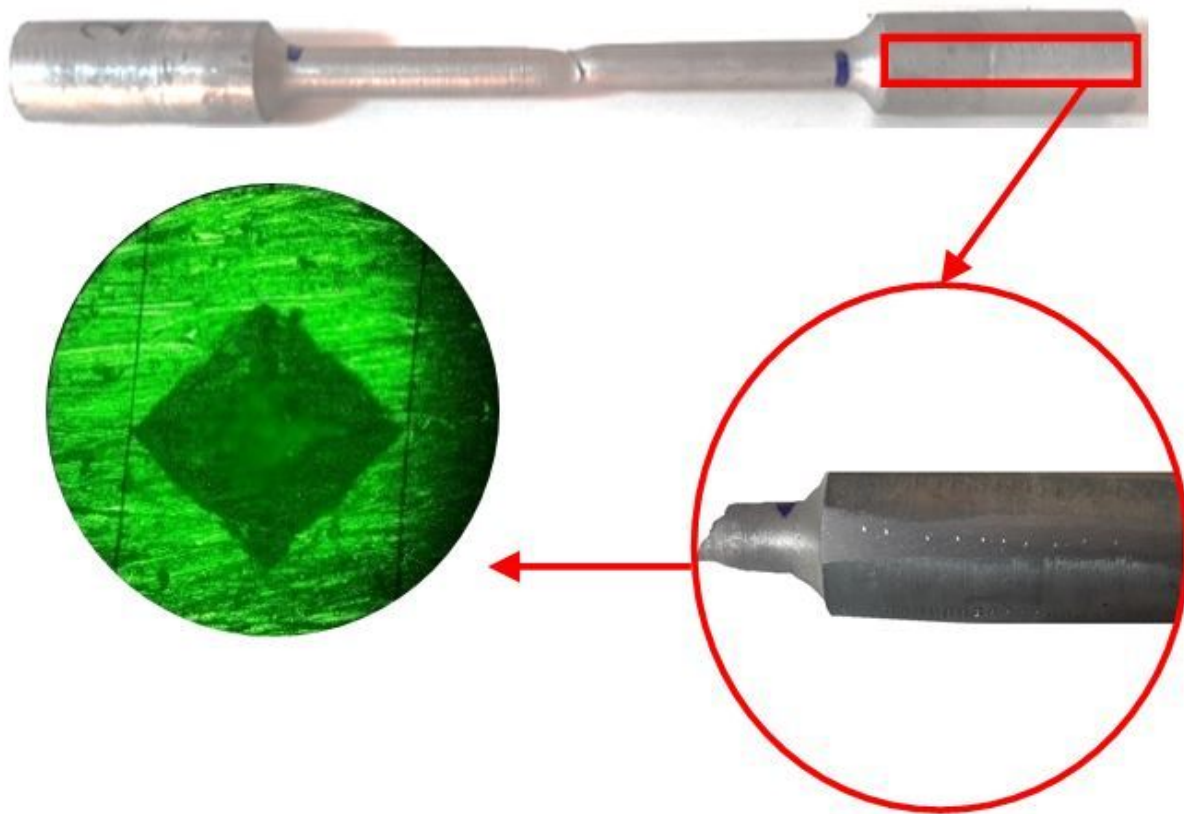
**Figure 3**

The measurement points for hardness

**Figure 4**

Hot forging press and tooling
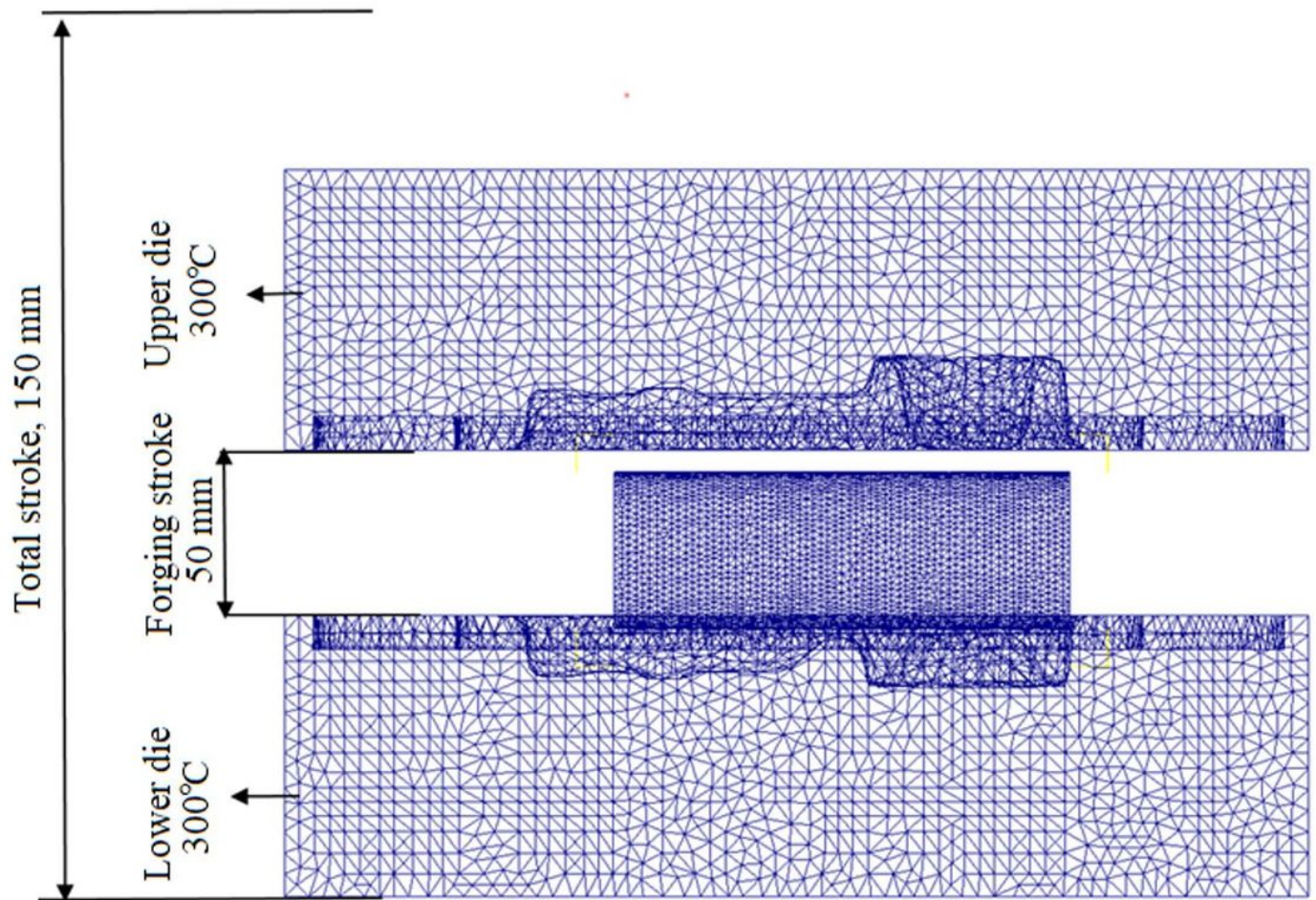
**Figure 5**

A finite element model of the hot forging process
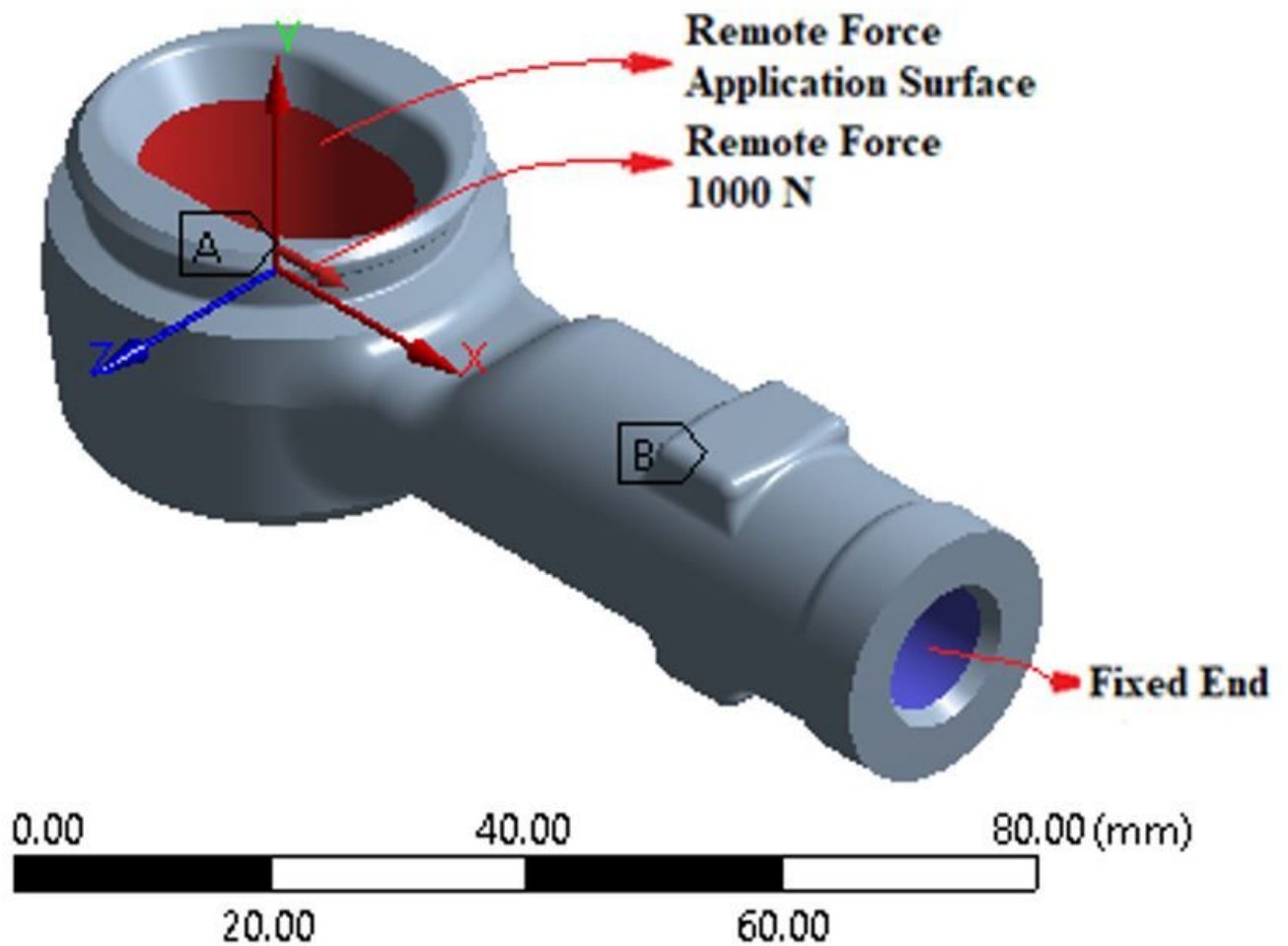
**Figure 6**

A finite element model for the fatigue simulation
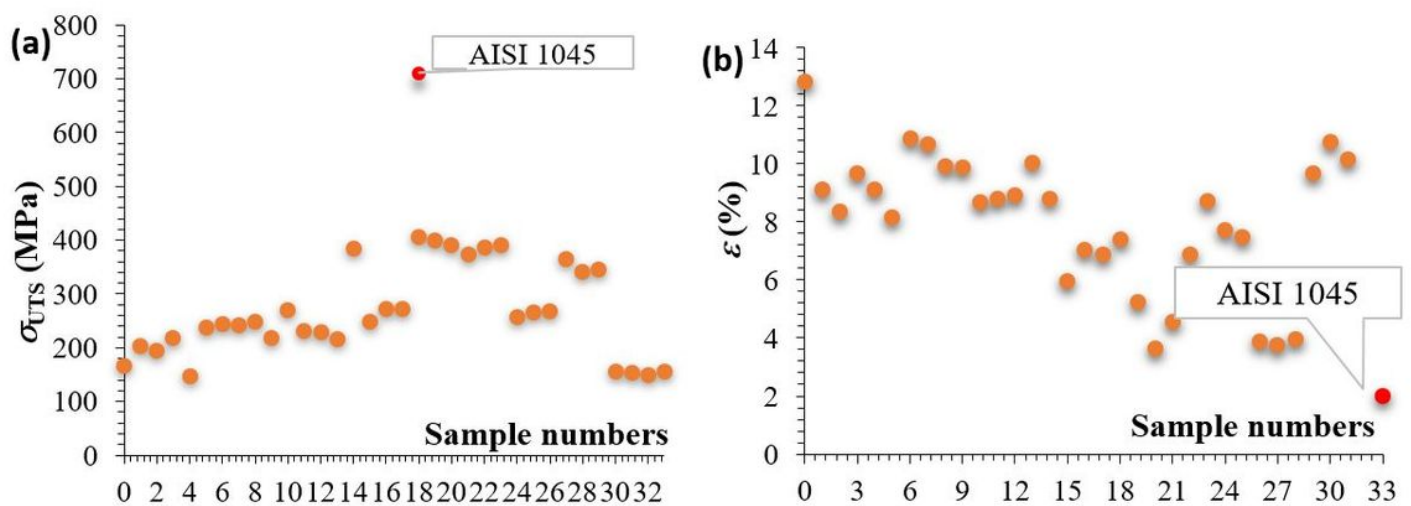


**Figure 7**

(a) UTSs and (b) strains at break of the AA6082 samples
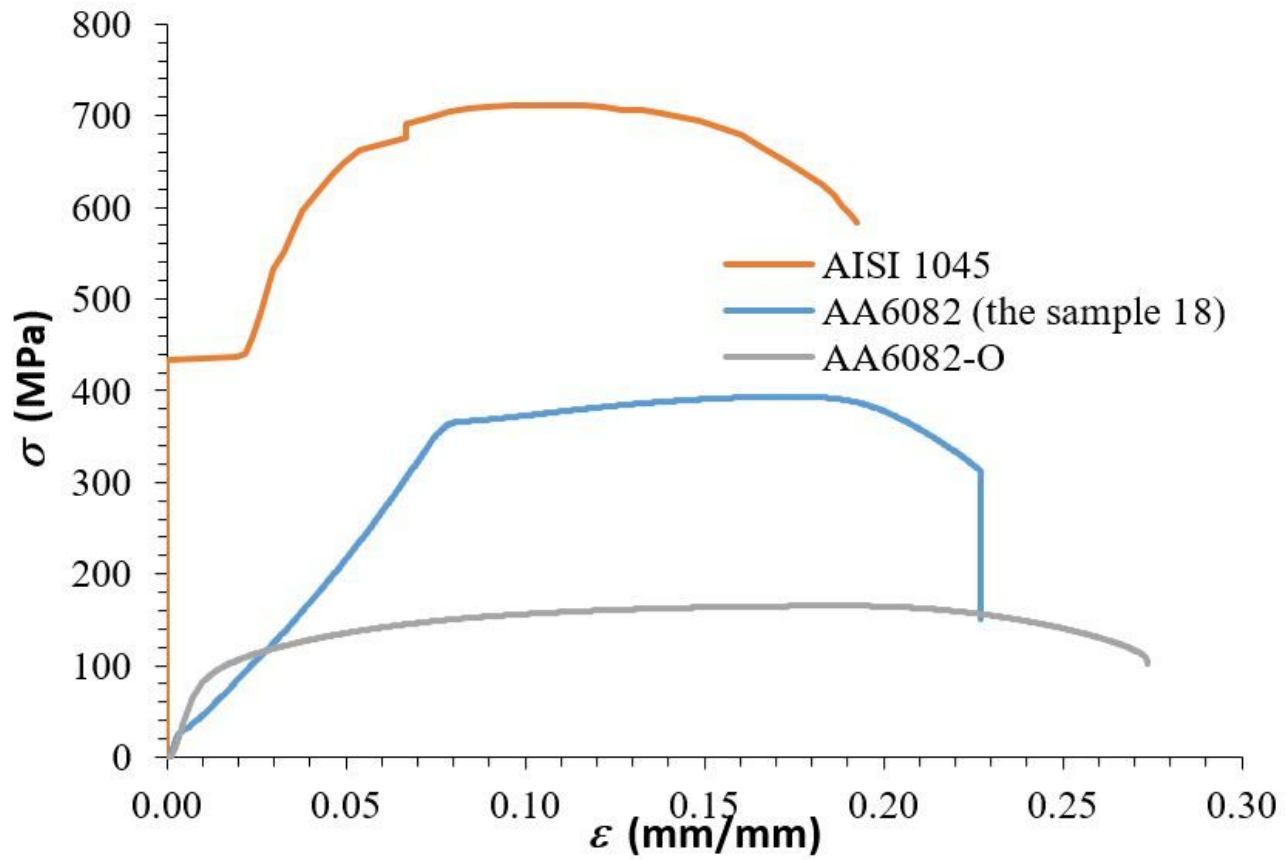


**Figure 8**

Comparison of engineering tensile curves of AA6082 and AISI1045
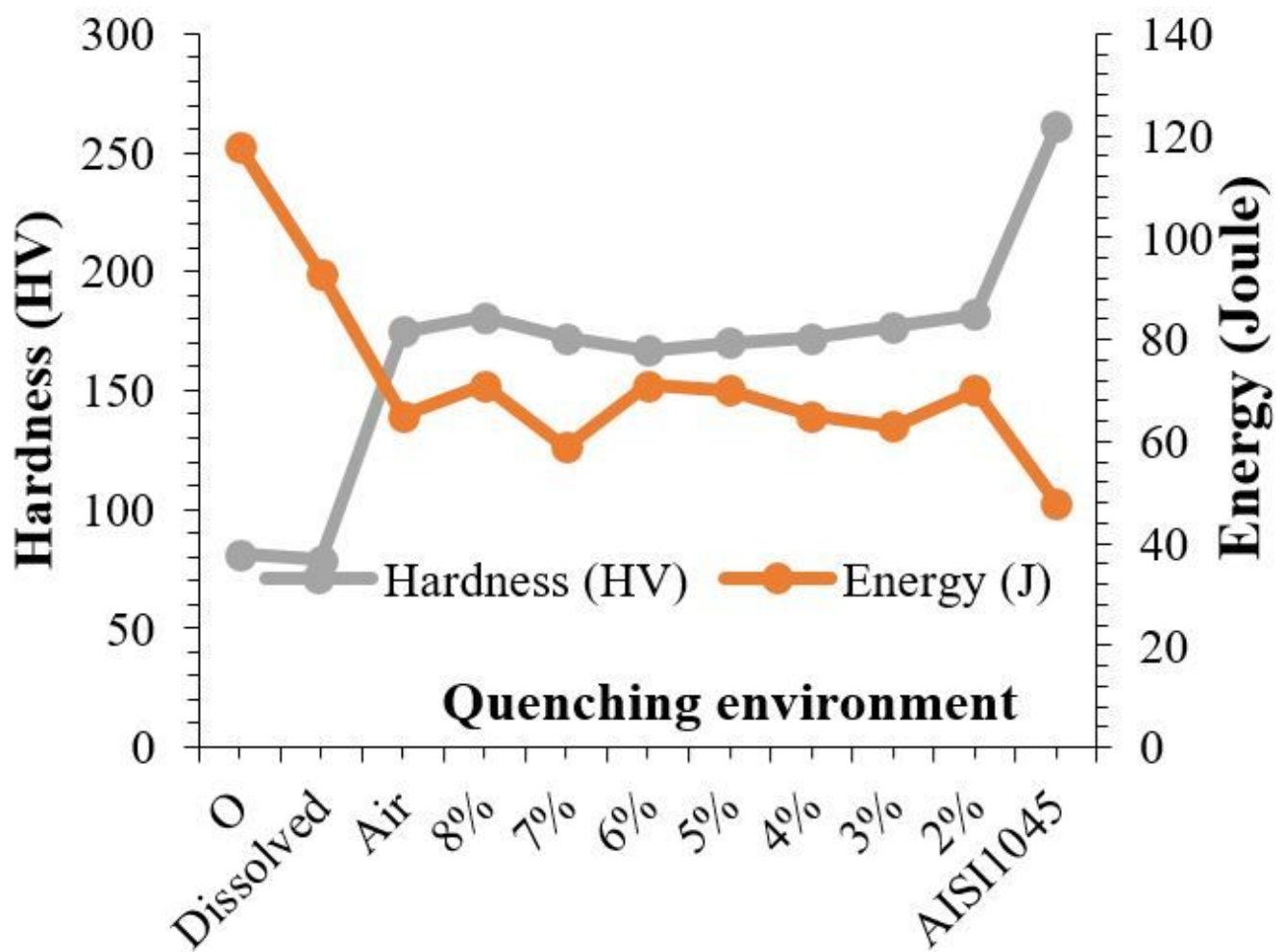
**Figure 9**

Hardness and Charpy impact energy
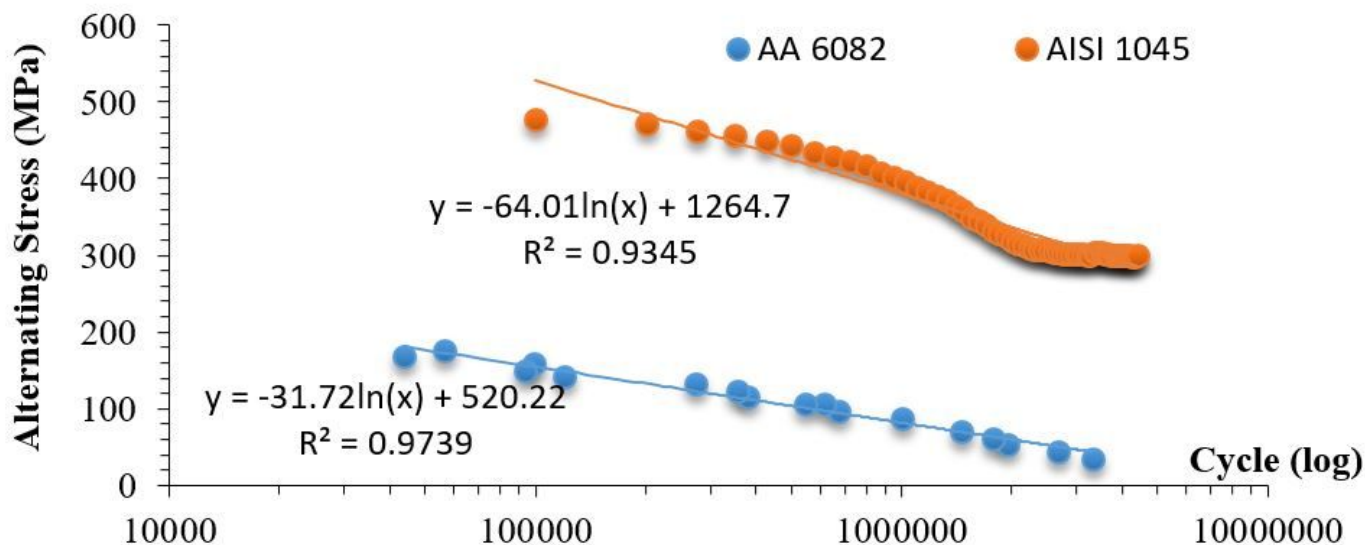
**Figure 10**

Wöhler curves of AISI1045 and the specimen 18
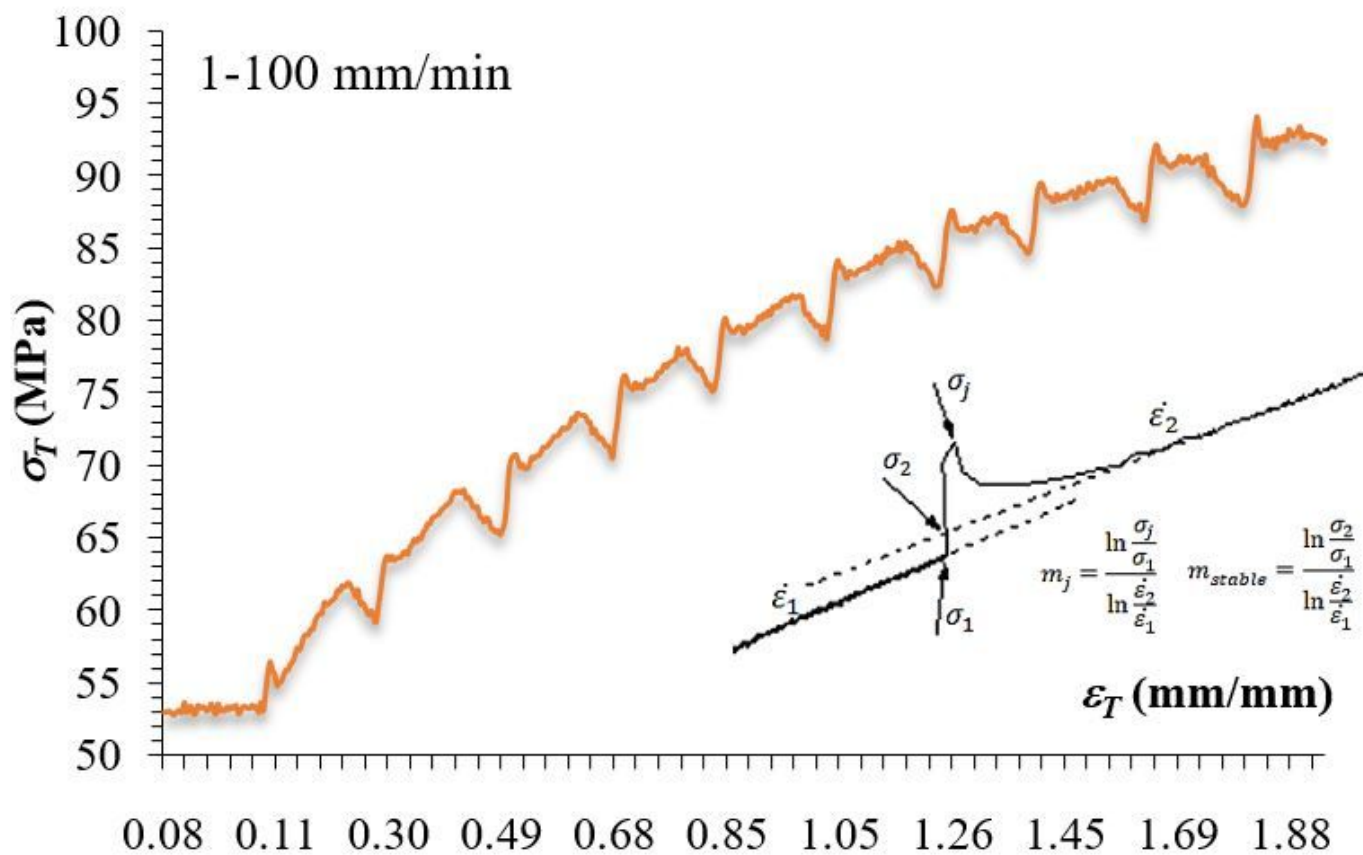


**Figure 11**

Jump test curve
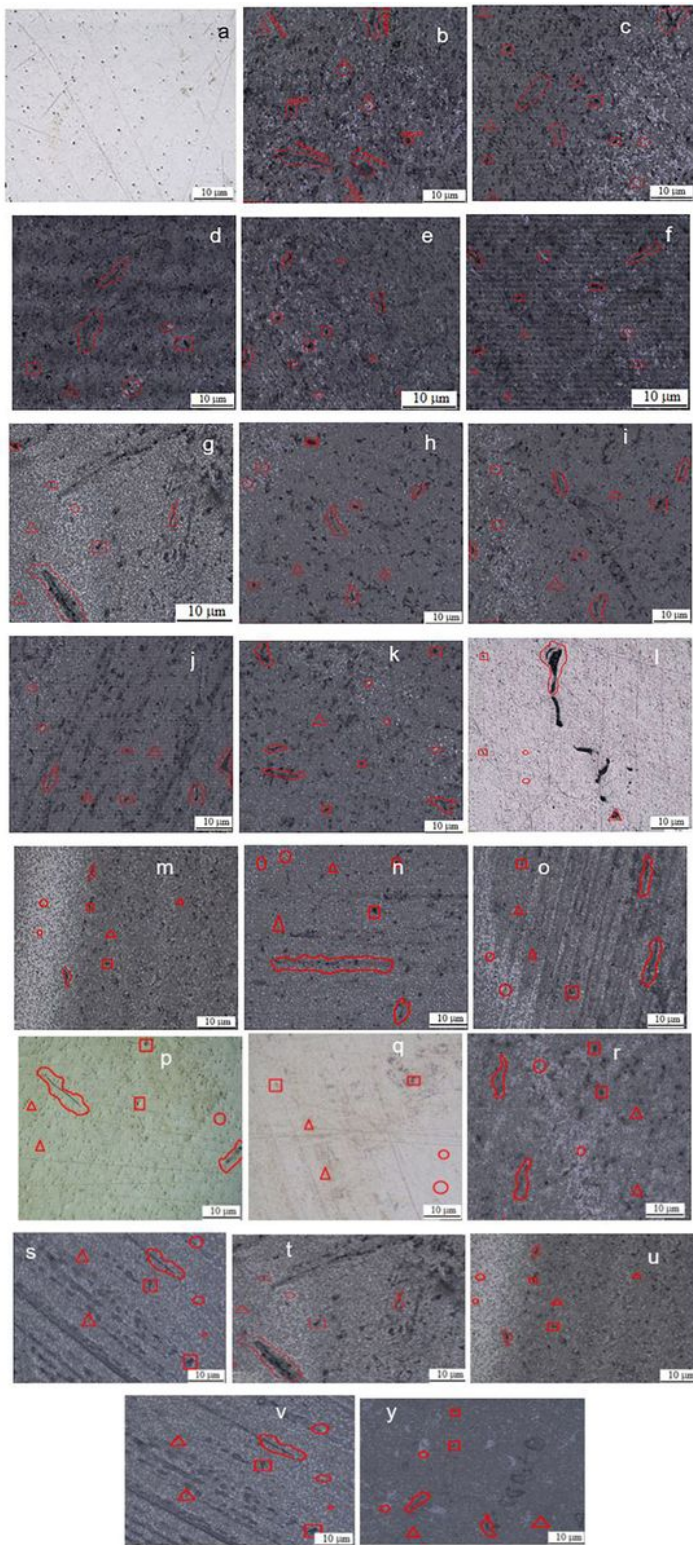


Figure 12

Optic examinations a AA6082-O b water quenching, 2 h aging at 175°C c water quenching, 4 h aging at 175°C d water quenching, 8 h aging at 175°C e water quenching, 10 h aging at 175°C f water+50%polymer mix quenching, 10 h aging at 175°C h water quenching, 2 h aging at 185°C i water quenching, 4 h aging at 185°C j water quenching, 6 h aging at 185°C k water quenching, 8 h aging at

185°C l water quenching, 10 h aging at 185°C m water+50%polymer mix quenching, 10 h aging at 185°C n: water quenching, 2 h aging at 195°C o water quenching, 4 h aging at 195°C p water quenching, 6 h aging at 195°C q water quenching, 8 h aging at 195°C r water quenching, 10 h aging at 195°C s water+50%polymer mix quenching, 6 h aging at 195°C t water+50%polymer mix quenching, 2 h aging at 175°C u water+50%polymer mix quenching , 4 h aging at 185°C v: water+50%polymer mix quenching, 6 h aging at 195°C y: water+50%polymer mix quenching, 10h aging at 220°C.



Figure 13

The hot forging of the rod end at elevated temperatures
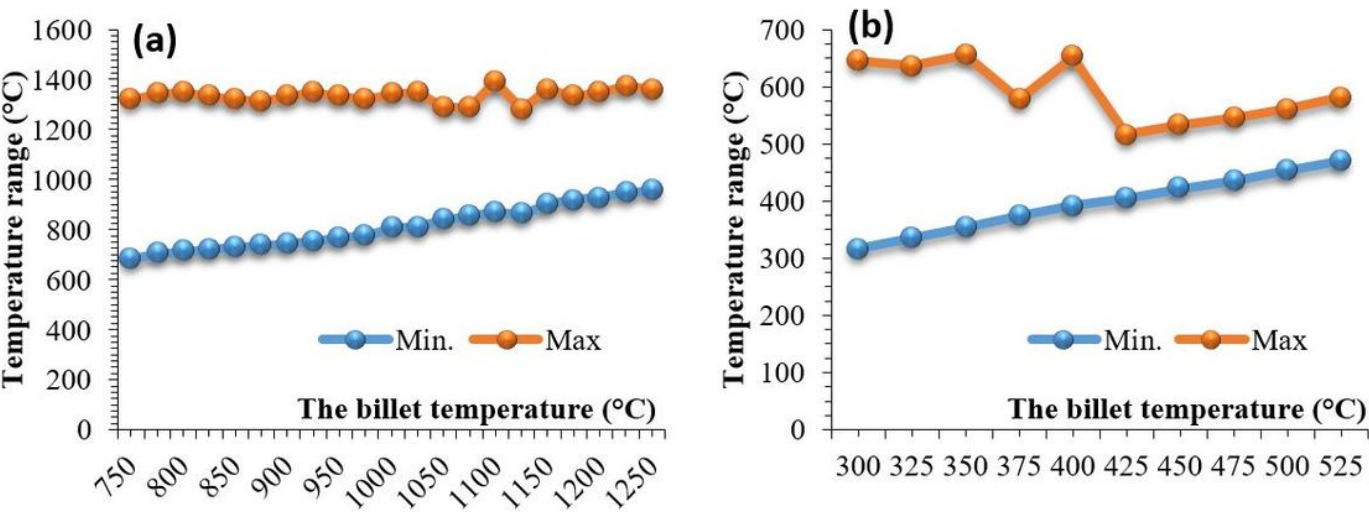


Figure 14

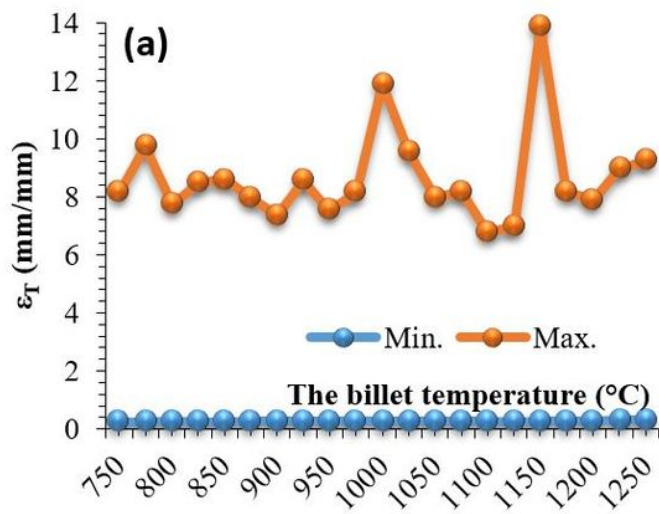The billet temperature ranges during the hot forging of (a) AISI1045 and (b) AA6082
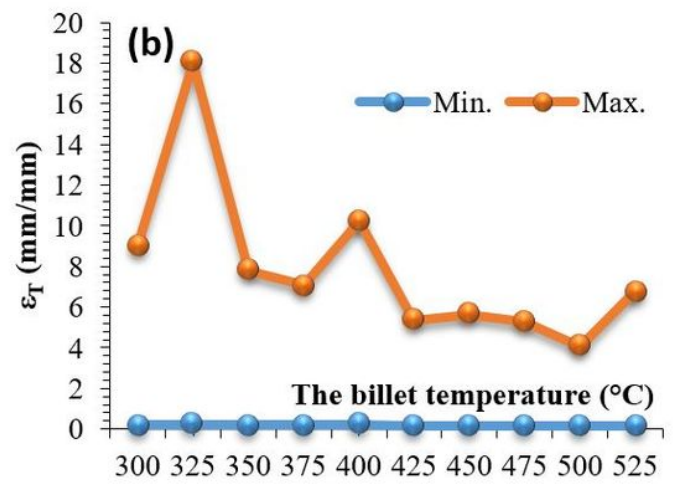
Figure 15

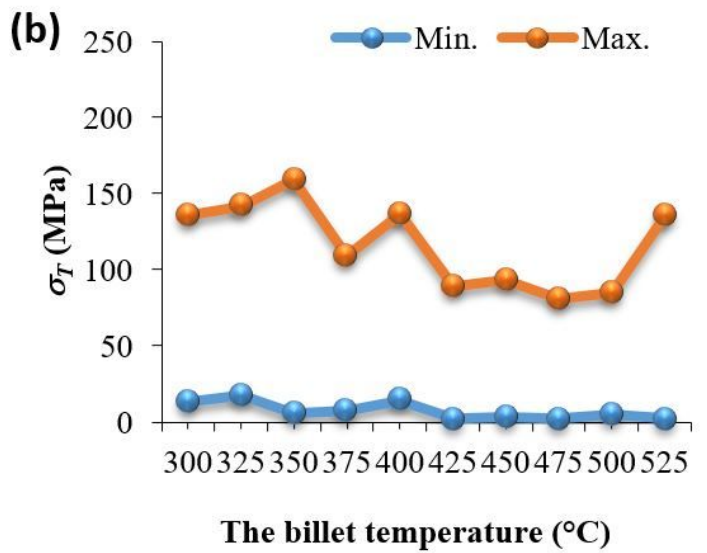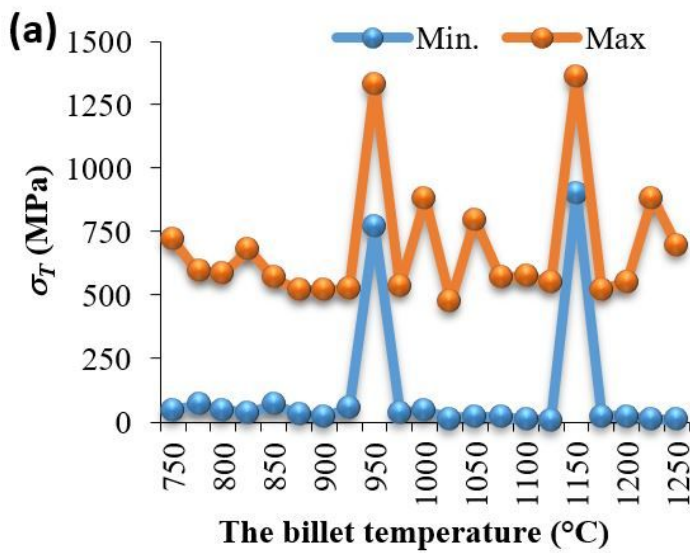The strain in the hot forging of (a) AISI1045 and (b) AA6082



Figure 16

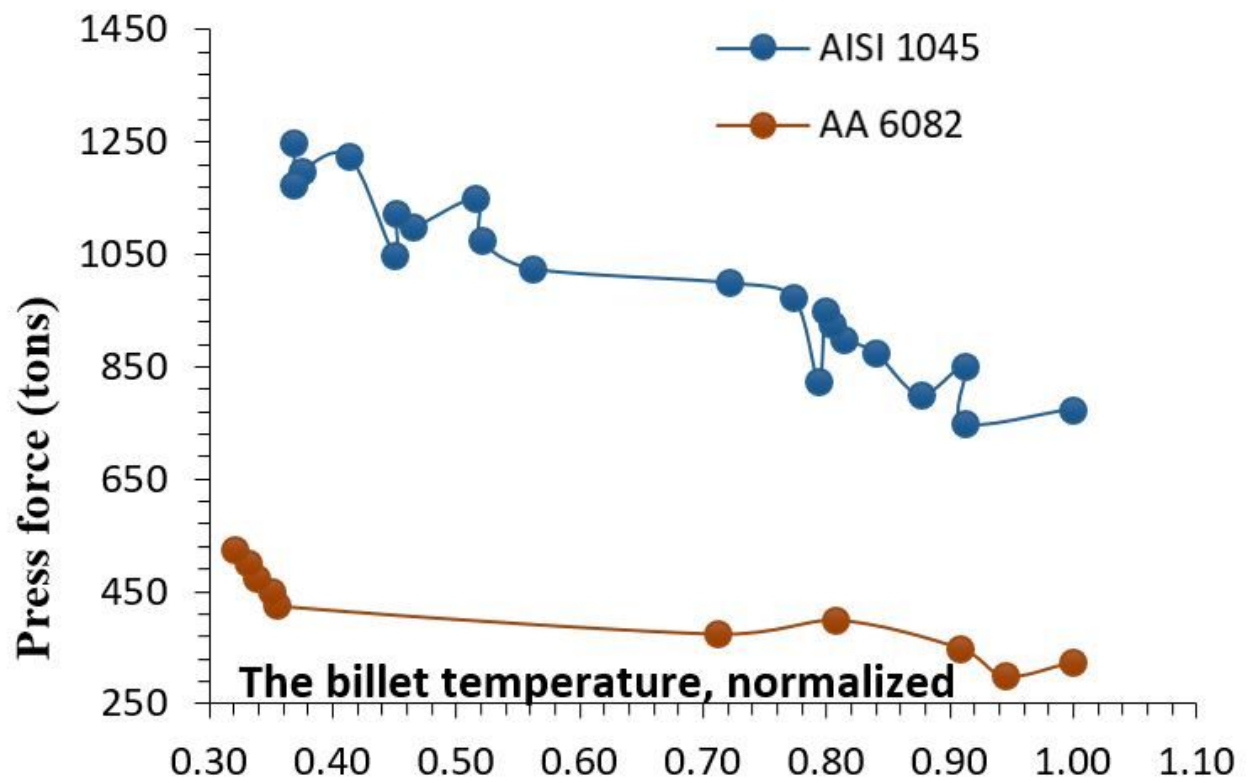The stress in the hot forging of (a) AISI1045 and (b) AA6082
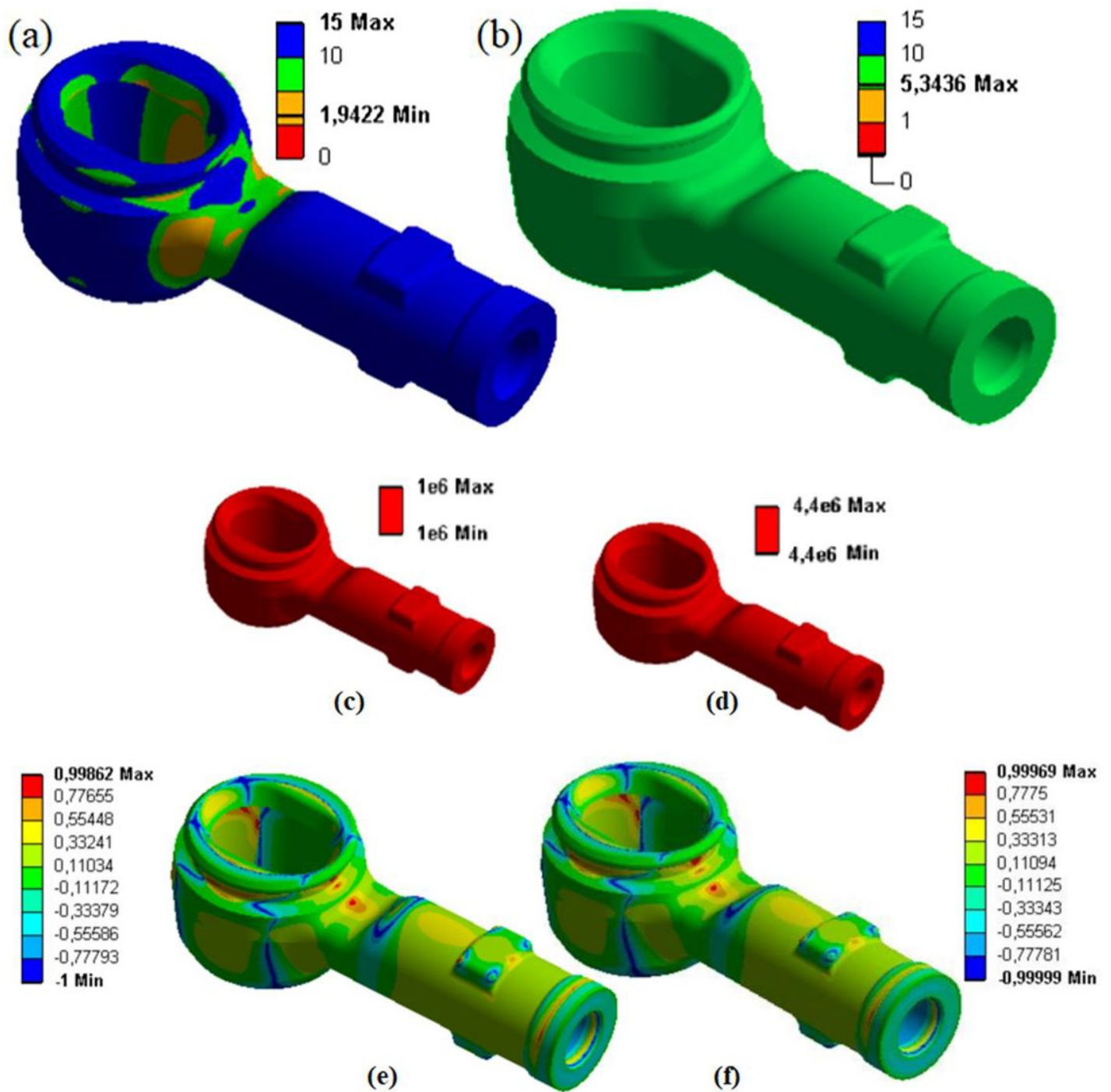
**Figure 17**

Press force requirements

**Figure 18**

Safety factor solutions (a) for AA6082 (b) for AISI1045. Service life (c) for AA6082 (d) for AISI1045. Biaxial stress solution (e) for AA6082 (f) for AISI1045
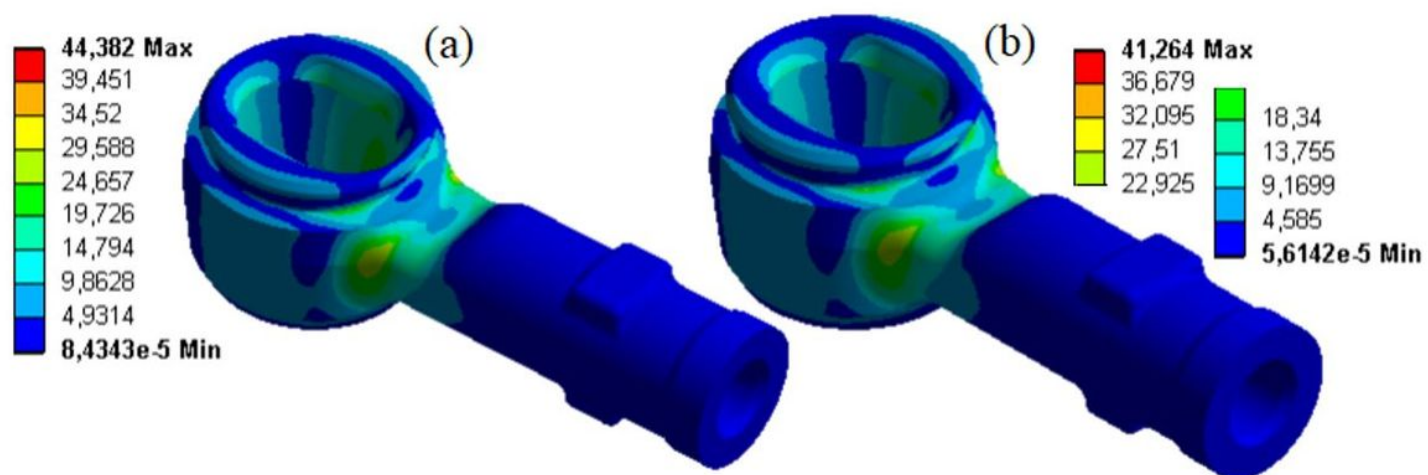
**Figure 19**

Stress solutions (MPa) (a) for AA6082 (b) for AISI1045

## Supplementary Files

This is a list of supplementary files associated with this preprint. Click to download.

- Investigationof.pdf